DANISH METEOROLOGICAL INSTITUTE

SCIENTIFIC REPORT

02 - 12

SAR Ice Classification
Using Fuzzy Screening Method

December 2002

Rashpal S. Gill

dmi.dk

Copenhagen 2002

PREFACE

A semi-automatic SAR sea ice classification algorithm is described. It is based on combining the information in the original SAR data with those in the three 'image' products derived from it, namely Power-to-Mean Ratio (PMR), the Gamma distribution and the second order texture parameter entropy, respectively. The technique used to fuse the information in these products is based on a new method called Multi Experts – Multi Criteria Decision Making (ME-MCDM) fuzzy screening. The Multiple Experts in this case are the above four 'image' products. The two criteria used currently for making decisions are the Kolmogorov-Smirnov distribution matching and the statistical mean of the float values.

The main advantage of using this image classification scheme is that, like neural networks, no prior knowledge is required of the statistical distribution of the different surface types. Furthermore, unlike the methods based on neural networks, no prior data sets are required to train the algorithm. All the information needed for image classification by the method is contained in the individual SAR images and associated products.

The algorithm classifies an image into any number of predefined classes of sea ice and open water. The representative classes of these surface types are manually identified by the user. Further, as SAR signals from sea ice covered regions and open water are ambiguous, it was found that a minimum of 4 pre-identified surface classes (calm and turbulent water and sea ice with low and high backscatter values) are required to accurately classify an image. Best results are obtained when a total of 8 surface classes (2 each of sea ice and open water) in the near range and a similar number in the far range of the SAR image are used.

Initial results illustrating the potential of this ice classification algorithm using the RADARSAT Scan-SAR Wide data are presented and its possible extension to fuse the information in these data with the ENVISAT ASAR image products is also discussed.

Keywords: SAR, KS Distribution Matching, Ice Cover Classification, Fuzzy Rule, Fuzzy Screening Method, ME-MCDM, RADARSAT, ENVISAT ASAR, Greenland.

List of contents

1. Introduction

In recent years satellite image classification and multi sensor data fusion based on neural networks (NN) and fuzzy set theory have received much attention in the open literature (Zadeh, 1965, Kohonen et. al., 1995, Masselli et. al., 1995, Atkinson and Tatnall, 1997, Chanussot et. al., 1999, Solaiman et. al., 1999, Tupin et. al., 1999, Andrefouet et. al., 2000, pal et. al., 2000, Tupin et. al., Melgani et. al., 2000, Wu and Linders, 2000, Moore et. al., 2001, Zhang and Foody, 2001). One of the main reason why NN has gained popularity over the more traditional statistical approaches is that the former is distribution free i.e., no prior knowledge of the distribution(s) underlying the different surface classes are needed for classification, only the actual data. There are several different types of NN and one thing they all have in common is that they all require the training of the network (Atkinson and Tatnell, 1997). The training can be supervised or un-supervised. The supervised training algorithms include those based on Multi-Layer Perceptron (MAL) using feed - forward concept and those using the feed – back neural network, for example the so-called Hopfield network (Atkinson and Tatnell, 1997). In these algorithms prior data sets of known classes are required. In the case of MAL, the training of the network involves the fine tuning of the weights of the connections, while in the case of the Hopfield network, the output from the nodes are fed back into the input. In the unsupervised training network no prior information is provided about the desired classification, the network learns itself so to speak. The Organising Topological Map is an example of this type of unsupervised network (Atkinson and Tatnell, 1997).

In the neural network approach a given unknown pixel or a region is classified into one of the pre-defined classes. In other words, a given pixel is either a full member of a particular class or is not a member. This is one of the disadvantage with using a NN approach, as in many cases data are mixed i.e., an unknown pixel may partially belong to several classes as the boundary between them may not be sharp. Fuzzy set theory explore this concept. In the fuzzy classification schemes, a given pixel can partially belong to several classes. In this case the contribution of each class in the pixel or a region must be estimated. Some of the most well known algorithms based on fuzzy theory are the hard and fuzzy-c means (HCM, FCM) clustering algorithms used for image segmentation (Pal et. al., 2000). Since its first introduction by Zadeh (1965), fuzzy set theory has invaded into many other fields beside fuzzy classifications, which include fuzzy control systems, fuzzy image processing (Melgani et. al., 2000).

Recently, neuro-fuzzy techniques have been developed which make use of both neural networks and fuzzy concepts (Atkinson and Tatnell, 1997).

All three of these fields have evolved much in the last two decades, the interested reader should refer to the above references for further details.

This report concerns the evaluation of a new fuzzy classification scheme, called the fuzzy screening method, which is used in here to classify RADARSAT ScanSAR images of the waters around Greenland into sea ice and open water regions. In particular, the main goal was finding an optimal method to fuse the information in the original SAR image with that contained in the image products derived from it, namely, Power-to-Mean Ratio (PMR), Gamma probability distribution function (Gamma-pdf) and the second order texture parameters such as entropy (Gill, 2001, 2002, Gill and Valuer, 1999). All these derived products contain additional, complementary, information, which in many cases is helpful in discriminating between the different surface cover types (Gill, 2001).

The particular fuzzy screening method that has been used is called Multi Experts – Multi Criteria Decision Making (ME-MCDM). The method is originally due to Yager (1993) and "*is useful in environments in which we must select, from a large class of alternatives, a small subset to be further investigated*". As far as known to the author this method has not been used for image classification before. It has been chosen because it is well suited for fusing the information from multiple sources such as mentioned above; amplitude, PMR, Gamma-pdf and entropy image products. In this scheme, and like neural net-

works, no prior knowledge is required of the underlying statistical distribution of the different surface types. Furthermore, unlike the neural network approach, no prior data sets are required to train the algorithm. All the information needed for image classification by the method is contained in the individual SAR images and associated products. The manual identification of the training surface classes is required.

This article essentially consists of three sections. In the next section, the ME-MCDM method is outlined. In chapter 3 the adoption of the ME-MCDM scheme for SAR image classification scheme is described. Results of applying the method to classify the SAR images are given in chapter 4. Finally, chapter 5 consist of discussion and conclusion.

2. ME-MCDM Fuzzy Screening Method

This method is applicable to those situations in which one has some preliminary information about the possible solutions, called *alternatives* in fuzzy terminology, and one has multiple judges, called *experts*, which by applying multiple *criteria* can filter out the most likely solutions for further analysis or screening. These screening problems form part a ME-MCDM (Multiple Experts – Multi Criteria Decision Making) problem with minimal information. The latter complicates the fuzzy problems because it limits the operations which can be performed in the aggregation processes needed to combine the multi-experts as well as multi-criteria. The fuzzy screening procedure developed by Yager (1993) can be used in many different types of problems such as pattern recognition, medical diagnosis and financial decision making. In this report it is applied to SAR image classification.

Below the most important elements of this method that are relevant for the classification of the SAR images into different regions of sea ice and open waters are summarised. For further details the reader should refer to Yager (1993) and Fuller (1996).

The fuzzy screening method developed by Yager is a 2 stage process.

1. In the first stage, individual experts are asked to provide an evaluation of the alternatives.

2. In the second stage, using fuzzy set theory rules, the individual experts evaluations are aggregated to obtain an overall value for each alternative.

The problem consists of 3 components.

A. A collection of all alternative solutions, X

$$X = \{X_1, X_2, \ldots\ldots, X_p\} \tag{1}$$

where p is the total number of possible solutions or alternatives. In the case of the problem being addressed in here this refers to the total number of possible classes of open water and sea ice types identified by the user in a SAR image and its associated products.

B. A group of judges, or experts, A

$$A= \{A_1, A_2, \ldots\ldots, A_r\} \tag{2}$$

where r is the total number of experts which in this present are 4: the amplitude SAR image and the 3 products derived from it: PMR, Gamma-pdf and entropy (ENT).

C. The third component is a collection of criteria, C

$$C= \{C_1, C_2, \ldots\ldots, C_n\} \tag{3}$$

where n is the total number of relevant criteria used by the experts to evaluate the alternatives. In the present case C is set at 2. The first criteria used is the Kolmogorov-Smirnov (KS) statistical test in which distributions of the unknown regions in the 4 image products are matched with those of the training classes determined manually. The second criteria employed is using the statistical means of the unknown and known classes and comparing their difference.

Stage 1: Rating of each alternative by each of the expert

Thus for each alternative/solution an expert is asked to evaluate how well that alternative satisfies each of the criteria in the set C. These evaluation can be given in linguistic terms as illustrated in the table below:

Outstanding (OU)	S_7
Very High (VH)	S_6
High (H)	S_5
Medium (M)	S_4
Low (L)	S_3
Very Low (VL)	S_2
None (N)	S_1

Thus for each alternative an expert provides a collection of n values, one for each criterion

$$P = \{P_1, P_2, \ldots\ldots, P_n\} \tag{4}$$

where P_j, is the rating of the alternative on the j-th criterion by the expert. Each P_j, is the element in the set of allowable scores, S.

Independent of this evaluation of alternative satisfaction to each criterion, each expert must associate a measure of importance to each criterion using the same scale, S.

The next step in the process is to find the overall valuation for an alternative by a given expert. To do this a negation of the importance of the criterion is required which is

$$Neg(S_i) = S_{q-i+1} \tag{5}$$

where q is the highest score possible. Then the unit score for each alternative by each expert, denoted by X_{ik} is given as follows

$$X_{ik} = Min_j[Neg(I_i) \grave{} P_j] \tag{6}$$

where $\grave{}$ denotes a maximum operation and I_j denotes the importance of the j-th criterion. The above equation can be seen as a measure of the degree to which an alternative satisfies the proposition *"all criteria are satisfied."* It can be seen as a generalization of a weighting averaging. Linguistically the formulation is saying that *"if a criterion is important then an alternative must score well on it"*.

At the end of the first stage one has for each alternative a collection of evaluations

$$\{X_{i1}, X_{i2}\ldots\ldots, X_{ir}\} \tag{7}$$

where X_{ik} is the unit evaluation of the i-th alternative by the k-th expert.

Stage 2: Combining experts ratings

In this section the rating for each alternative by the different experts are combined to obtain an overall evaluation for each alternative. To do this the Ordered Weighted Averaging (OWA) operator is used. Further it is *assumed that each of the expert have the same importance.* In the present SAR image classification, this means all 4 products, AMP, PMR, GAMMA-pdf and ENT are independent of one another and are of equal importance. This assumption is not strictly valid as the 3 latter products (PMR,

GAMMA-pdf and ENT) are also derived from the original SAR and the reader should bear this in mind. However, this assumption will be satisfied in the future when the ENVISAT ASAR and RADARSAT data are used together for image classification. One of the reasons why the fuzzy screening method described here has been considered for SAR image classification in the first place is because of its flexibility to fuse data from different sources or sensors.

In this section an aggregated function Q, which can be seen as a generalisation of the idea of how many experts it feels need to agree on an alternative before it is accepted to pass through the screening process. The value Q(i), where i=1 to r, is an indication of how satisfied i experts, out of a total of r, are in passing an alternative. The value Q(i) should be drawn from the scale $S=\{S_1, S_2, S_3, \ldots\ldots, S_n\}$ described above. Q(i) has the following characteristics.

1. As more experts agree the decision making confidence should increase.

    $Q(i) = Q(j)$, $i > j$.

2. If all experts are satisfied then the confidence should be highest.

    $Q(r) = perfect$.

The function Q can take different forms depending on the importance the user wish to assign to the number of experts that must first agree before the alternative is accepted. A function that emulates the average is denoted by Q_A and is defined for all i=0, 1, ...r as

$$Q_A(k) = S_{b(k)} \tag{8}$$

Where

$$b(k) = Int[1 + (k.\frac{q-1}{r})] \tag{9}$$

where q is the number of points on the scale, S mentioned above, k=0, 1, ..., r, and Int is an operator returning the integer value that is closest to the float number in the square bracket in the equation above.

Having appropriately selected Q then one is in a position to use the OWA method for aggregating the expert opinions.

The first step in the OWA procedure is to order the X_{ik}'s in descending order which is denoted by B_j, which is j-th highest score amongst the experts for the i-th project.

The overall evaluation for the i-th alternative is then calculated from the following equation

$$X_i = Max_j[Q(j) \; ´ \; B_j] \tag{10}$$

Where ´ denotes the minimum. The Max operator plays a role similar to summation in the usual numerical procedure.

To appreciate the above formulation, B_j, can be seen as the worst of the j-th top scores, Q(j) as an indication of how important the user feels about the support of at least j experts. The term $Q(j) \; ´ \; B_j$ can be seen as a weighting of a alternative's j best scores, B_j, and the decision maker feel that j experts have confidence in the alternative.

Finally, hard classification of a given unknown region in a SAR image is then deduced in the defuzzyfi-cation step by taking the maximum of the alternatives given by equation (10).

In the following chapter, it is described how the fuzzy screening method outlined above is adopted for SAR image classification.

3. ME-MCDM Applied to SAR Image Classification

As outlined in the previous section, the three components of the ME-MCDM are the *experts*, possible solutions called *alternatives* and a set of *criteria* used by the experts to give ratings of each alternative. What each one of these three components are in relation to the classification of a SAR image into different regions of open water and sea ice is outlined below.

1. *Experts*: In the present case these are the following 4 image products (floats) which are obtained from the original RADARSAT ScanSAR Wide 8-bit, 100 m pixel size, 500 km wide swath width (approximately 100 Mbytes), amplitude data.

   - **AMPLITUDE (AMP)** product obtained by averaging window of size 4×4 pixels, and fixing the distance between two of these consecutive windows at 4 pixels in both directions.

   - **GAMMA-pdf** product computed using the following probability distribution for the average intensity of m pixels, $\bar{I}$ (Gill, 2002):

$$P_g(\bar{I}) = \left(\frac{mL}{m_B}\right)^{mL} \frac{\bar{I}^{(mL-1)}}{\Gamma(mL)} \exp\frac{-mL\bar{I}}{m_B} \tag{11}$$

   where L is the number of looks, Γ is the Gamma function and m_B is the mean intensity of the background. The size of window and inter window spacing used to compute GAMMA-pdf is same as for the AMP.

   - **Power-to-Mean ratio (PMR)** product computed using the following expression

$$PMR = \frac{<I^2>}{<I>^2} \tag{12}$$

   where I is the intensity value, for window size of 20×20 pixels, with inter spacing of two consecutive windows again fixed at 4 pixels in both directions.

   Finally,

   - **ENTROPY (ENT)** which is the second order texture parameter derived from the Grey-Level Co-occurrence Matrix (GLCM) (see, for example Gill, 2001) computed using the expression:

$$ENT = \sum_j \sum_i - P_{ij} \log(P_{ij}) \tag{13}$$

   where P_{ij} is a square matrix which is the count of the number of occurrence of two neighbouring pixels, at two different locations within a square window of size W*W

which have grey values i and j. To compute ENT the 8 - bit SAR data was reduced to a 6-bit product and window sizes were same as for PMR.

The averaging of windows is necessary to compute the products and to reduce the background speckle noise by smoothing the data. Further this has the advantage of reducing the data volume of each image product used in the evaluation and hence shorten the computation times.

2. *Alternatives* refer to the number of different classes of water and sea ice into which the SAR images are to be classified. Obviously there is a minimum of 2 (one each for water and sea ice). In fact this is one of the parameters that is explored in this report, namely, the minimum number of classes of water and sea ice of different ice concentration needed to capture the essential information in a SAR image to satisfy operational ice charting needs. Consideration also has to be given to the fact that the SAR signals of open water and of sea ice are ambiguous and further the grey tone values of the same surface class can be different in the near and far range of the image. In this report the number of classes are varied from a minimum of 2 to a maximum of 12 (6 each for open water and sea ice). For example if the total number of classes are eight, then the SAR image is classified into the following classes:

  a. Calm water (of the type) in the near range of the SAR image,
  b. Turbulent water in the near range,
  c. Calm water in the far range,
  d. Turbulent water in the far range,
  e. Sea ice of low concentration in the near range,
  f. Sea of high concentration in the near range,
  g. Sea ice of low concentration in the far range,
  h. Sea ice of high concentration in the far range.

Then during the fuzzy screening each unknown region of a SAR image is classified into one of these 8 alternatives. The 2 classes of each surface type from the near and far range are then combined together to give 4 final classes. Further discussion of the number of alternatives and their distribution are given in the next chapter.

The way the training areas of the different classes are determined manually for the 4 products have been described previously (Gill, 2002). Very briefly it involves the following 2 steps.

i) Training areas of different surface types (e.g., calm and turbulent water, sea ice of low and high concentration, multi- and first- year sea ice, and if appropriate sea ice in different stages of development, etc.) are generated by displaying the AMP product on a computer terminal (SILICON GRAPHICS ERDAS IMAGINE work station). In particular, regions of size ˜ 20 × 20 pixels of different surface types are manually identified in the AMP image. This creates the mask file, example of which is shown in figure 2 which shows the mask file superimposed on top of the AMP image. In the figure a total of eight regions (4 each of water and ice) have been manually identified. In practice there is no limit to the number of different regions of open water or sea ice of different concentration or type that can be chosen for image classification.

ii) The mask file generated above is then used to identify and store in a buffer the data points pertaining to different surface types from each of the four products: AMP, GAMMA-pdf, PMR and ENT. These are the data points within the colour boxes shown in figs. 2 - 5.

3. *Criteria*. As mentioned in the last chapter currently 2 criteria are used for making decision by the experts. These are Kolmogorov – Smirnov (KS) distribution test in which the statistics of the un-

known region of an image are compared with those of known classes determined manually as outlined above. The advantage in using the KS test is that a prior knowledge of the respective distribution of the known and unknown classes is not needed. The KS test simply determined whether the 2 data sets belong to same distribution or not (Gill, 2002). Thus the KS test is used to match the data points in each of the four experts to their respective data points pertaining to a different surface type to determine the probabilities of a match (perfect match: probabilities = 1.0, no match: probabilities = 0.0). To compute these probabilities a test window of size 4×4 pixels, which was determined by carrying out trials with windows of different sizes and was found to be both computationally optimal and statistically sufficient, is slid across the four products (Gill, 2002). The pixels in these 4×4 test windows are compared with the pre-determined surface classes using the KS test to determine whether the two data sets belong to the same distribution.

The second criterion is based on comparing the statistical means of the unknown and known classes. This is one of the parameters i.e., the grey tone values, used naturally by human operators to discriminate between the different surface types in an image. Other criteria can also be included such as the second moment of the pdf (variances) and criteria based on geometrical features of sea ice floes and so on. These are not reported in here.

The above 2 criteria are used by the experts to give ratings i.e., scores, to each class of open water and sea ice for a given test window on a scale of 1 -10.

3.1 Why use fuzzy screening method for image classification.

Finally a summary of the reasons why the ME-MCDM procedure has been adopted to classify SAR images are listed below.

1. Possible to have multiple experts. This translates into fusing data and products from different sources, including sensors.

2. Possible to classify an image into any number of different classes (alternatives).

3. Possible for the user to define the multiple criteria in the decision making.

4. Flexibility to associate importance to each criterion i.e., *"if a criterion is important then an alternative must score well on it."*

5. Allows the user the flexibility to alter, if necessary, how many experts have to agree before an alternative is accepted for further screening.

3.2 Computational procedure.

1. Compute the 4 float image product (AMP; GAMMA-pdf, PMR and ENT) as outlines above.

2. Manually identify on a computer screen the number of classes of open water and of sea ice into which the SAR image is to be classified. Store the float values of these different classes.

3. By using a 4×4 test window in each of the four products, compute the scores of each of the above class for each of the above 2 criteria.

4. Use the fuzzy screening rules to aggregate the scores for each class from each of the 4 products for the test window using equation (10). This will result in the overall scores for each class for the test window.

5. Hard classify the overall scores for the test window by de-fuzzying the results. This is achieved for the time being by taking the class that has the maximum overall score.

6. Steps 3 – 5 are repeated for the entire image by sliding the above 4 × 4 window across the image.

The overall SAR image classification based on the fuzzy screening method described above is shown in figure 1 below.

SAR Classification using fuzzy screening method
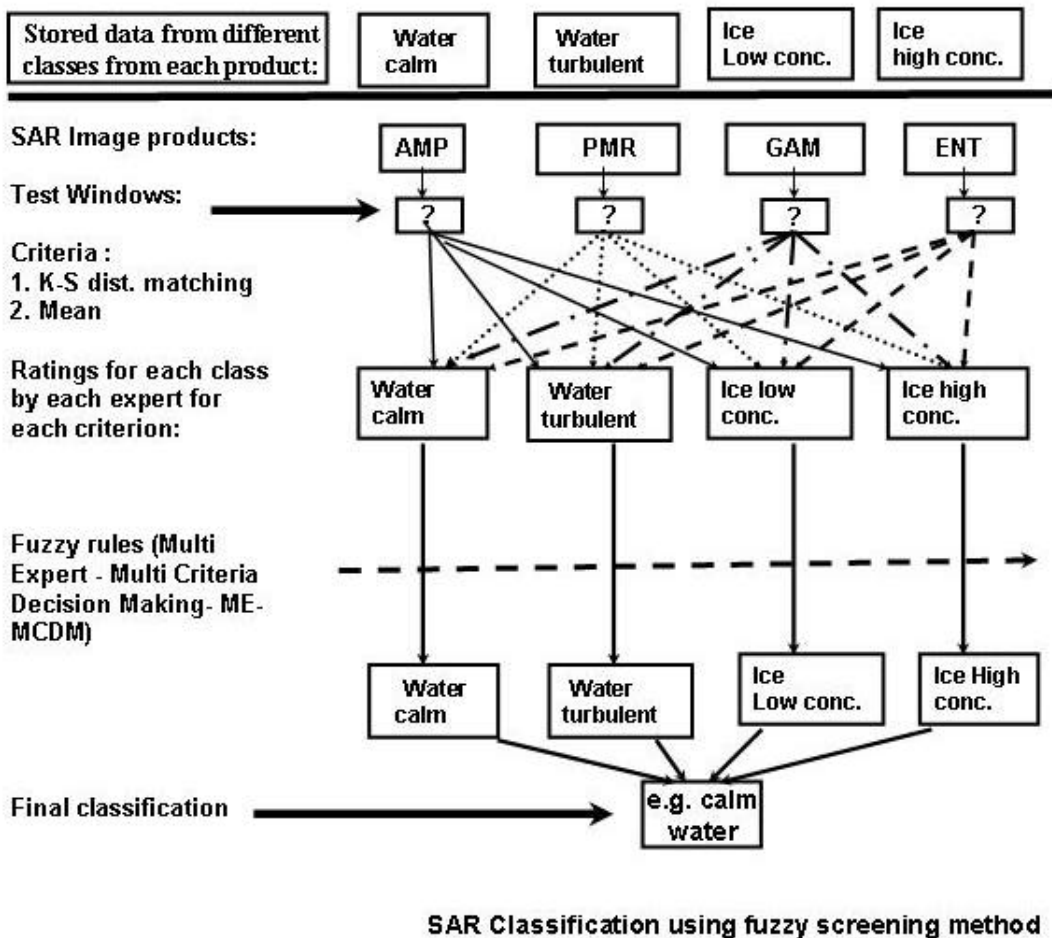
Figure 1. Shows the sketch of the SAR image classification using the fuzzy screening method. In the figure the number of alternatives are 4 (calm and turbulent water and sea ice of low and high concentration), number of experts are also 4 (AMP, PMR, GAM (=GAMMA_pdf) and ENT). The 2 criteria used are the KS and the statistical means.

4. Results

This consists of, for the purpose of illustrating the method, a classification of two RADARSAT Scan-SAR Wide images shown as figures 2 and 23, respectively, and given at the back of this report. The first image is from Disco Bay region of West Greenland from 2000-05-24. This image has been chosen because it is relatively easy to interpret manually and thus is adequate for illustrating the results. In particular, this image contains essentially 3 surface types: first year ice, fast ice and open water all of which are indicated on the figure. The second SAR image is much more difficult to interpret. It contains many different surface types: sea ice of both very low and very high concentration, calm and turbulent open water regions and first and multi-year sea ice floes, as indicated on the figure. This second image is of Scoresby Sound from the East coast of Greenland from 2000-07-22.

In both figures 2 and 23 typical regions, representative of different surface types are indicated by different colour boxes and have been marked with a unique identity code (e.g., I-1 and W-1). These regions were manually identified as described in the last chapter. For example, fig. 2 contains 8 boxes, 2 each of red, yellow, blue and turquoise. In particular, red and yellow boxes indicate regions of sea ice of low and high backscatter values while blue and turquoise boxes indicate calm and turbulent open water regions. Similarly, fig. 23 contain 12 boxes, three each for sea ice (low and high ice concentration) and open water (calm and turbulent water) from the near, middle and far ranges of the RADARSAT image. The data points from four different products (AMPLITUDE, GAMMA, PMR and ENT) within these (and only these !) boxes are stored in a buffer and are used in the two criteria (KS distribution matching test and a comparison of the mean values) of the fuzzy image classification scheme described in the last section. The results from this image classification scheme are presented below.

4.1 RADARSAT image from West Coast of Greenland

Figures 3 - 5 show the PMR, GAMMA and ENT 'image' products, respectively, on a grey tone scale, after appropriate scaling, corresponding to the AMPLITUDE image product shown in figure 2. All 3 of these figures shows the usefulness of these products for interpreting the original SAR image (fig. 2) (Gill, 2002).

Below the results of image classification using the above fuzzy screening method with 2, 4 and 8 alternative (surface classes) are presented below.

4.1.1 Number of surface classes 2

4.1.1.1 Maximum number of 2 experts

Figure 6 shows the classification of the RADARSAT image using only: (i) the AMP expert, (ii) KS criterion and (iii) just two alternatives (one each of water and ice with the identities W-4 and I-3, respectively). As can be seen from this figure the classification of the different regions of sea ice and open water seems to be reasonably accurate. There are few in-accuracies in this classification such as some of the first year ice floes (and the ice region between them) with low grey tone values have been misclassified as water. This is indicated on the figure. The results presented in fig. 6 are nothing more than the KS probabilities obtained by matching the unknown pixels with the predetermined water and sea ice pixels. The fuzzy screening method plays essential no role because only one expert has been chosen to do the screening and there is nothing to aggregate. Further, as in this case there are only 2 classes to choose from, fig. 6 simply shows when the AMP pixels in the test windows lies closer to either the predetermined class of water or sea ice. The results , nevertheless, shows the potential of the classification method using just 2 classes.

The results shown in fig. 6 should be seen as only those of the expert AMP who was allowed to use only one criterion and given just 2 alternatives to chose from. Figure 7 shows the results of the classification when we have 2 experts (AMP and PMR). All other parameters in the fuzzy screening were identical as in fig. 6 above. In this figure one can see that combining the individual classification of the experts AMP and PMR have not resulted in improved image classification. Instead the results are inferior to those in figure 6 where the opinion of the expert AMP only were sought. In particular, comparing figs. 6 and 7 one can see that many more first year ice floes and the ice between them have been misclassified as water. Further the fast ice region (top-middle of the image) has also been misclassified as water.

To understand this, it should be pointed out that the default class of the test window as been set as water. The consequence of this is that in the case when the 2 experts, as in this case, disagree with one another about the classification of the test window then that window automatically gets classified as water. It should be noted that when the 2 experts disagree with one another then there is 50% : 50% chance the class of the window in question is either water or ice. Thus the extra regions of open water in fig. 7, when compared to fig. 6, should been be interpreted as the test windows for which the experts AMP and PMR were in disagreement (as to their class type).

From a statistical point of view PMR is a measure of regions heterogeneity. Then the fact that more of the ice regions are misclassified as water means that the PMR values are not sensitive enough in some regions to discriminate between the two classes. This can be ascertained by manually inspecting PMR grey tone image shown in fig. 3. The PMR parameter is useful for delineating surface boundaries, icebergs and the structures, such as ice ridges, with ice floes.

Figure 8 shows the classification of the image carried out by the experts AMP and GAMMA. Again all other parameters were same as for fig. 7. Comparing this figure with figs. 6 and 7 discussed above, it can be seen that the results of the image classification by the experts AMP and GAMMA are very similar to those obtained using the expert AMP alone. In particular, comparing fig. 8 with fig. 6 shows that few more of the ice region have been misclassified as water (especially the fast ice region at top middle of the image). The reason for this are the same as for fig. 7 above i.e., extra regions of open water within the ice areas should again be interpreted as the test windows for which the experts AMP and GAMMA were in disagreement. The fact that the result of the evaluation by the experts AMP and GAMMA (fig. 8) are not too different from those obtained by using expert AMP alone (fig. 6) implies that these 2 experts are mostly in agreement about classifying the different regions of the SAR image.

Similarly, figure 9 shows the results of the classification carried by the experts AMP and ENT. As can be seen from this figure that combining the evaluations by the expert ENT with those of AMP alone has not improved the image classification. In particular, some of the ice regions are again misclassified as open water. The reasons for this are same as above i.e., these are the ice regions when the experts AMP and ENT have been in disagreement. More specifically, the correctly classified ice regions obtained by using only expert AMP in fig. 6 which are now misclassified as water in fig. 9, results because of the misclassification by ENT. The reason for this is that the entropy values of many of the ice and water regions are very ambiguous.

The overall conclusion to be drawn from the results presented in fig. 6 – 9 above is that combining the evaluations of the results obtained by either of the experts PMR, GAMMA or ENT with those of AMP alone does not lead to improved image classification. The reason for this is only 2 experts and 2 surface classes have been used in the fuzzy model and when the experts disagree with one another then software model just assigns a default class (water) for the test window in question. In the next section results of aggregating the evaluations by 3 or more experts including using 2 criteria are presented.

4.1.1.2 Maximum number of 4 experts

Figure 10 shows the results of the image classification obtained by aggregating the results from the 3 experts AMP, GAMMA and PMR. The criterion and the surface classes used were again identical with those used in the previous results. As can be seen from this figure the image classification is much more realistic. Further, some of the characteristics of what GAMMA and PMR products measure are now reflected in these results. In particular, some of the small regions of ice and icebergs in the open water between land on the east and first year ice on the west, are now also properly classified. To understand how combining the scores from both GAMMA and PMR with those from AMP have improved the overall image classification while it lead to poorer results when only GAMMA or PMR were aggregated with AMP one has to recall that this is the weighting of an alternatives 3 scores with the measure of confidence expressed by the function Q(j) (equation (9)). This means for any test window at least 2 experts are always in agreement as to which class it should belong. Thus the 50% : 50% uncertainty in the cases above when only 2 experts were used and when they disagree does not arise in this case.

Figure 11 shows the results when aggregate the evaluations of 4 experts (AMP, PMR GAMMA and ENT). All other parameters were same as in fig. 10 above. As can be seen from this figure the results are much worse than when only 3 experts were used. Some of the misclassified areas are indicated on the figure. The reason for the misclassification results when the judges do not have a majority verdict i.e., 2 of the experts says it is ice while the other 2 says it is not (i.e., it is sea ice). In these cases the test window in question is assigned the default class which is water.

Instead of using the KS criterion the reliability of using instead the statistical mean values was also investigated. The results are shown in figs. 12 and 13, respectively. In particular, in fig. 12 the number of experts are 3 (AMP, PMR and GAMMA) while in fig. 13 all 4 experts are used. The number of alternatives are again only 2; the same water and ice classes used in figs. 6 – 11 above. Comparing figs. 12 and 13 with their counterparts, figs. 10 and 11 one can see that the results obtained using the mean values criterion are much inferior than those obtained using the KS criterion. This leads to the obvious conclusion that the mean values criterion is not as effective as the KS test at discriminating between the water and sea ice classes.

Figures 14 and 15 shows the results of aggregating the findings of the 3 experts AMP, PMR and GAMMA using both of the criteria (KS and the mean values tests). The classes of water and sea ice are same as above. In fig. 14 the 2 criteria have been assigned same importance while in fig. 15 KS test has been given higher importance because of the above results in figs. 12 and 13. From these results it can be seen that the results presented in fig. 15 are now much more accurate than those in fig. 14. These results shows the flexibility of the fuzzy screening model presented here i.e., allowing for unequal importance to the decision making criteria.

The results presented in figures 16 and 17 are obtained using the same parameters as used in figs 14 and 15 above, respectively, except now all 4 experts (AMP, PMR, GAMMA and ENT) are used in the decision making. The conclusions to be drawn here are thus the same as those obtained for figs. 14 and 15, namely by assigning less importance to the mean values criterion results in improved image classification.

The effect of using different classes of open water and sea ice in computing the scores in the KS and mean values criteria was also investigated and the results are shown in fig. 18. In this case all the parameters were identical to those used for fig. 17 except now the water and sea ice pixels designated by W-3 and I-4 (instead of W-4 and I-3 used in fig. 6 – 17) were used. The position of these different classes are shown in fig. 2. Comparing figs. 17 and 18 it can be seen that the final image classification is also sensitive to the actual regions of water and ice used for matching in the 2 criteria. From this one can draw the obvious conclusion that the representative classes of the different surface types must be chosen with care.

In the above examples the maximum number of pre-determined classes used for computing the scores in the 2 criteria have been 2 (one each of water and sea ice). In the following section results are presented when a total of 4 (2 each of water and sea ice) pre-determined classes are used in the classification.

4.1.2 Maximum number of surface classes 4.

Figures 19 and 20 shows the results of using 4 pre-determined classes of open water and sea ice for classifying the SAR image. In particular, in both figs. 19 and 20 the 4 water and sea ice classes designated by W-3, W-4, I-3 and I-4 were used which represent a class of (i) calm water (W-3), (ii) turbulent water (W-4), (iii) ice with low backscatter (I-4), and (iv) sea ice of high backscatter (I-3). These are the classes used for image classification in figs. 6 -17 and fig. 18. As in fig. 16 – 18, more importance was given to the KS distribution matching criterion than to the mean values criterion. Then the results shown in fig. 19 were obtained using the experts AMP, GAMMA and PMR. In fig. 20, on the other hand, all 4 experts (the above 3 and ENT) were used. It can be seen from figs. 19 -20 that the quality of the image classification has significantly improved. In particular, the different regions of calm and turbulent water and that of sea of low and high backscatter values have now been differentiated. The classification on the whole appear to be much more representative of the different classes of open water and sea ice present in the image.

The effect of using only 3 and all 4 experts can also be deduced by comparing figs. 19 and 20. The obvious difference is that in fig. 20 there are more ice floes with higher backscatter values and some of the water regions classified as calm in fig. 19 and now classified as turbulent water. Qualitative comparison of figs. 19 – 20 with the original RADARSAT image and the AMP image product shown in fig. 2 shows that fig. 20 is a more accurate representative of the 4 different surface classes than fig. 19.

4.1.3 Maximum number of surface classes 8.

Finally, figs. 21 – 22 shows the results of image classification when a total of 8 pre-determined classes of calm and turbulent water and sea ice with low and high backscatter values were used. In particular, these were 2 classes each of calm water (W-1, W-3), turbulent water (W-2, W-4), sea ice with low backscatter values (I-1, I-3) and with high backscatter values (I-2, I-4). Again in fig. 21 the experts AMP, GAMMA and PMR were used while in fig. 22 all 4 were used. Comparing the results presented here with those in the previous section above it can be seen that there is less difference between figs. 21 – 22 than their counter parts figs. 19 – 20. In particular, there appears to be very little difference between the classification of the open water regions in figs. 21 – 22, implying that the opinion of the additional expert (ENT) was not too different from those used in the classification shown in fig. 21. However there is some difference between the classification of the sea ice regions in figs. 21 and 22. In particular, in fig. 21 some parts of ice floes in the left of the image and parts of the fast ice region at top middle have been misclassified as turbulent water, both of which are indicated on figure. The conclusion to be drawn from this is that using more test classes of water and sea ice in the fuzzy classification scheme does not necessarily results in more accurate image classification. Thus the final judgement of the quality of the image classification must be left to the user.

Comparing figs. 21 and 22 shows that using 4 experts, instead of only 3, has resulted in improved image classification.

The image used above to illustrate the potential of the fuzzy screening method is relatively easy to interpret manually. The performance of this fuzzy method used to classify a much more complex RADARSAT image are given below. This image is from the East coast of Greenland, off Scoresby Sound at ˜ 70 °N from 22nd July 2000.

4.2 RADARSAT image from East Coast of Greenland

Figures 23 - 25 shows the 3 experts, AMP, GAMMA and PMR shown on a grey tone scale used in the classification. These image products were computed in the same way as figs. 2 -4 above. In particular, in fig. 23 a total of 12 classes (3 each of calm and turbulent water and sea ice of low and high backscatter values) were manually identified. Of these the pairs (W-1, W-2) and (I-1, I-2) represent calm and turbulent water and sea ice of low and high backscatter in the near range of satellite pass (right half of the image as indicated on the figure). Similarly (W-3, W-4) and (I-3, I-4) are their counterparts in the far range of the image. The pairs (W-5, W-6) and (I-5, I-6) are the representative classes of these 4 surface types in the middle part of the image. As in the previous section these 12 alternatives, 3 experts and the 2 decision making criteria were used in the image classification. Further the effect of only using representative classes from the near or far range was also investigated. These results are discussed below. To help the reader assess the accuracy of these results, some of the important regions in the image, such as the turbulent water region in the near range, ice of high concentration in the far range, a multi-year ice floe in the mouth of Scoresby Sound have been indicated on fig. 23.

The pair of figures 26 – 27 shows the results of image classification when the pre-determined classes from the far range (fig. 26) and near range (fig. 27) were used in the 2 decision making criteria. As can be seen from these figures, the results of image classification are significantly different. In particular, the turbulent water region in the near range has been totally misclassified in fig. 26. Similarly many of the water regions have been misclassified as sea ice in fig. 27. On the whole it can be seen that with the exception of misclassifying the turbulent water region in the near range as sea ice with low backscatter (colour code red), the results shown in fig. 26 are reasonably accurate. This cannot be said of the results shown in fig. 27. From this one can conclude that the representative classes of water and sea ice from the near range are much worse than their counter parts from the far range in the fuzzy image classification scheme used here. These results in some sense were expected because the backscatter from the near range are characterised by steep radar incidence angles which are known to be poor for sea ice open water discrimination as has been found previously during the evaluation of ERS-SAR imagery (Gill et. al., 1995).

Figure 28 shows the results of image classification using a total of 8 representative classes of water and sea ice (4 from the near range and a similar number from the far range of the image). Only the expert AMP and one criterion (KS distribution matching test) was used in the decision making. As can be seen from the results shown in the figure there are many regions that are misclassified some of which are indicated on the figure. In particular, the misclassification of some the sea ice in the mouth of the Sound as turbulent water (colour code: turquoise) and the misclassification of the turbulent water region in the lower middle of the image as sea ice with low backscatter (colour code: red). From this it is clear that, due to the complexity of SAR image, using just 1 expert and 1 criterion is inadequate to classify this image accurately.

Figure 29 shows the results of image classification when the 2 experts AMP and GAMMA were used to classify the image. All other parameters were identical to those used in the previous figure. Comparing fig. 29 with fig. 28 it can be seen that there is in fact significant improvement in the resulting classification. For example most of the sea ice in the Scoresby Sound, including most part of the multi-year ice floe, is correctly classified. This is also true for the sea ice surrounding the ice pack in the bottom left of the figure (indicated by the abbreviation xx on the figure). The turbulent water region in the bottom middle of the image misclassified as sea with low backscatter values in the last figure is now on the whole is also correctly classified. However, despite these improvements there are still regions of the image which are not correctly classified, especially the turbulent water in the near range (left hand side of figure) which is still misclassified as sea ice (colour code: yellow).

Similarly, figure 30 shows the classification of the same image when all 3 experts (AMP, GAMMA and PMR) were used for decision making. Again all other parameters were identical to the previous figure, especially only the KS criterion is used. Comparing this figure with the 2 previous ones one can again immediately see the improvements in the final classification. It can be seen from this figure that apart from the turbulent water region in the near range still misclassified as sea ice (colour code: red) and part of the multi-year ice floe classified as turbulent water (colour code: turquoise), most of the regions in the SAR image are correctly classified. A possible explanation why part of the multi-year floe is still misclassified as turbulent water is that parts of its surface may have undergone melting and thus in the classification is treated as a water class. Another reason in support of this explanation is that the image in question is from summer (22nd July).

Figure 31 shows the classification by using the above 3 experts but in this case instead of using the KS distribution matching test to make decision, the criterion based on the statistical mean values of the different classes, was used. All other parameters were identical to previous figure. Comparing this figure with fig. 30 it can be seen that using the mean values criterion is not as effective as KS test for image classification in the fuzzy scheme, thus confirming the results obtained in the previous section.

Figure 32 shows the classification of the SAR image using all 3 experts and both criteria with less importance given to the statistical mean criterion. As can be seen from this figure the classification of the image appear to be on the whole correct and improved to the case when just the criterion KS test was used (fig. 30). The only region which is still misclassified is the open water region in the near range of the image which is still misclassified as sea ice (colour code: yellow). Also notice that some of region in fig. 30 have been reclassified from one sea ice class into another (colour code: from red to yellow). This is similarly true for the water regions.

Finally figure 33 shows the classification of the image when 12 predetermined test regions within the image are used in the image classification: In particular, these are the 8 classes used in the previous figures 28 – 32 plus 4 more; sea ice of low and high backscatter values and calm and turbulent water, from the middle part of the image. These 12 classes are marked on fig. 23 with the symbols I-1 to I-6 and W-1 to W-6 for sea ice and open water, respectively. Comparing figs 32 and 33 one can see that using 12 test classes of water and sea ice, instead of 8, has not improved the results significantly. More specifically, no region of water or sea ice in fig. 32 have been re-classified into another type. The changes are only, at best, re-classification of calm to turbulent water (colour code: red into turquoise) or sea ice with low backscatter to high backscatter (colour code: red into yellow), or vice-versa. The most disturbing result still is that the turbulent water region in the near range (left hand side of the image) is still misclassified as sea ice (colour code: yellow). The author has attempted using other representative surface classes of sea ice and water in the model, but to no avail.

5. Discussion and Conclusions

In this report a new fuzzy method called Multi Experts – Multi Criteria Decision Making (ME-MCDM) has been evaluated for classifying a SAR image into regions of calm and turbulent water and sea ice with low and high backscatter values. The desired aim of this investigation was to find a reliable method that would allow for the possibility of fusing the information in the SAR image with that in the texture and statistical image products derived from it. The latter products, described below, are found to contain useful supplementary information which is often useful during the manual interpretation of the images. The ME-MCDM screening method was selected as it was found to be very flexible with potential to include auxiliary information which could be relevant for image classification. In particular, it allowed for having multiple experts (the products), any number of image classes (called alternatives), possibility to use multiple weighted criteria. The scheme also allowed the user to determine how many experts had to agree before a test window was believed to be reliably classified.

The main advantage of using this image classification scheme over the more traditional ones is that, like neural networks, no prior knowledge is required of the statistical distribution of the different surface types. Furthermore, unlike neural networks, no prior data sets are required to train the algorithm. All the information needed for image classification by the method is contained in the individual SAR images and derived products. The method does rely on the user identifying the training classes manually.

The 4 experts used for image classification were the AMPLITUDE, GAMMA-pdf, PMR and EN-TROPY. The former 2 are computed from the original RADARSAT ScanSAR Wide image by averaging 4×4 windows (the inert-pixel spacing of these windows was also fixed at 4×4 pixels to reduce data volume). PMR and ENTROPY were computed using equations (11) – (12) using window sizes of 20×20 pixels (see chapter for further details) The criteria used for making decisions were the Kolmogorov-Smirnov (KS) distribution matching test which involved comparing the unknown and known classes to determined whether they belong to the same distribution or not, and comparing the first order statistical means of the 2 classes. During the evaluations it was found that the second criterion was not as effective as the first (KS) in discriminating between the different classes which then allowed the option of associating less importance to it. Furthermore, it must be pointed out that the KS test has its own limitations: (i) it is most sensitive around the median of the cumulative distribution function and less sensitive at the tail ends, and (ii) it cannot discriminate between all types of distributions, such as a distribution with 2 maximums.

The evaluation of the ME-MCDM fuzzy screening method was centred around classifying 2 RADAR-SAT images. The first one was easy to interpret (fig. 2) with well defined boundaries between the water and sea ice classes consisting of first year and fast ice along the coasts. The second image (fig. 23), on the other hand, was its complete opposite; it was characterised by sea ice consisting of a mixture of first and multi-year floes of different ice concentration and very turbulent open water regions. A summary of the results obtained using each one of these SAR images are given next.

The results of image classification into just 2 classes (one each of water and sea ice) are shown in figs. 6 – 18. Results of using just one expert (AMP) and one criterion (KS) are shown in fig. 6. These results are surprisingly very accurate and were computed to illustrate the potential of this classification scheme. Figs. 7 – 9 show the classification based on using the above expert and one of the other: PMR, GAMMA or ENT, respectively. The results in these figures show to what degree these experts agree or disagree with AMP which can be ascertained by comparing these figures with fig. 6. In particular, if any one of the results shown in figs. 7 – 9 are significantly different from fig. 6 then it can be concluded that the 2 experts were in disagreement. Fig. 9, for example, was not significantly different from fig. 6 thus implying the experts AMP and GAMMA were broadly in agreement. The results of combining the opinion of 3 and 4 judges are shown in figs. 10 – 11 and a general improvement in the result classification of the image can be clearly seen. The results of using the statistical mean values criterion, instead of the KS,

are shown in figs. 12 -13. By comparing these results with the previous ones it can be deduced that this criterion is not as effective at discriminating between the different classes. The results of using both of the above criteria and still only 2 alternatives are given in figs. 14 – 17. From these results it can be seen that the best results are those shown in fig. 15 which were obtained by associating less importance to the mean values criterion and by not using the ENT expert (to see this compare figs. 15 and 17). From this it can be concluded that not all products are equally efficient at classifying a SAR image and that it would be useful if the ME-MCDM model allowed for the possibility of assigning weighting to the experts. This facility is not available in the current version of the model and will be investigated in the future. Finally, fig. 18 shows the results of classifications using a different class of water and sea in the 2 criteria for making decisions. As can be seen from this figure the results are unfortunately somewhat sensitive to the actual representative classes of water and sea ice used in computing the scores.

Results for using 4 classes; calm and turbulent water and sea ice with low and high backscatter values, are shown in figs.19 – 20. As can be seen from these 2 figures, by using 4 classes results in a much more representative and realistic classification of the SAR image. Further improvement results when using 8 surface classes in the classification as shown in figs. 21 – 22.

The results of applying the fuzzy screening method to classify a complex SAR image are shown in figs. 26 – 33. In figs. 26 – 27 the sensitivity of image classification scheme to using pre-determined classes from the near and far range were investigated. It was found that using the classes to compute the scores from the far range were far better than from their counter parts in the near range of the image. This re-sults confirmed earlier findings, namely that for reliable discrimination between sea ice and water re-gions radar incidence angles = 30 ° should be used (Gill and Valuer., 1999). The results of using a total of 8 test classes of water and sea ice are given in figs. 28 – 32. Figs. 30 – 31, again confirm the relative accuracy of the 2 criterion at discriminating between the different surface types with KS again confirm-ing its prominence. Further, from these figures it can be seen that the best results are those shown in fig. 32 which were obtained using both of the criteria, with less importance to mean values criterion, and all 3 experts AMP, GAMMA and PMR. Finally fig. 33 shows the results obtained by using a total of 12 test classes of water and sea ice. Comparing this figure to fig. 32 it can be seen that it does not result in any significant improvement.

From the results presented in fig. 6 – 33 it can be concluded that a minimum of 4 classes of water and sea ice are adequate for classifying the different surfaces in a RADARSAT image of sea ice. Best results are obtained when using 8 such classes.

A point to note is that using 4, 8 or 12 classes in the classification have not been able to classify cor-rectly the turbulent water region in the near range of the SAR in fig. 23. The result is obviously disap-pointing and shows the limitations of the 2 criteria used in the decision making. It is difficult to see how a criterion using the information within the individual SAR image (based on statistical distributions or texture parameters) can help resolve this problem. The best way to improve the image classification would be to use information contained in data from other satellite sensors, particularly SSM/I and/or QuickSCAT and ENVISAT (and the sea ice products computed from them). More specifically, an auto-matic SAR image classification method has been developed which uses the above ME-MCDM fuzzy method together with the sea ice product based on the SSM/I – 85 GHz and the EUMETSAT SAF – OI (Satellite Application Facility on Ocean and Sea Ice) sea ice concentration. The particular advantages of this method is that the training areas of representative classes are no longer determined by the user; the algorithm locates such classes automatically. Initial results obtained from the algorithm looks promising and shall be reported in the near future.

The effectiveness of using surface types identified in one SAR image to classify a SAR image of the same (and different) region, from another day, was also investigated by the author. The results found were not very encouraging and thus were not presented in this report. The main reason for this is that the

different image classes are too sensitive to the radar incidence angles, i.e., their position in the across range direction. Another important reason is that the statistical characteristics of the surface classes can, in the time between the 2 images, undergo significant changes (due to meteorological conditions). This finding has consequences for the algorithms based on neural networks which require credible training sets of the different classes.

Finally it should be recalled that in the ME-MCDM model it is assumed that all experts are independent and have same importance. This assumption is not strictly satisfied as all the 4 products are derived from the same original SAR image. This point should be borne in mind by the reader when evaluating the results presented in the last chapter. However, with the imminent availability of ENVISAT -ASAR data, this assumption will be satisfied when the model is used to fuse these data with those of RADARSAT. Results of this investigation will be reported in the near future.

6. References

Andrefouet S., Roux L., Chancerelle Y., and Bonneville A., 2000, "A Fuzzy-Possibilistic Scheme of Study for Objects with Indeterminate Boundaries: Application to French Polynesian Reefscapes", IEEE Trans. Geoscience and Remote Sensing, vol. 38, no. 1, page 257.

Atkinson P. M., and Tatnall A. R. L., 1997, "Neural network in remote sensing", INT. J. REMOTE SENSING, vol. 18., no. 4, pp 669 – 709.

Bendjebbour A., Belignon Y., Fouque L, Samson V. and Pieczynski W., 2001, "Multisensor Image Segmentation Using Dempster-Shafer Fusion in Markov Fields Context", IEEE Trans. Geoscience and Remote Sensing, vol. 39, no. 8, page 1789.

Chanussot J., Mauris G., and lambert P., 1999, "Fuzzy Fusion Techniques for Linear Features Detection in Multitemporal SAR Images", IEEE Trans. Geoscience and Remote Sensing, vol. 37, no. 3, page 1292.

Fuller R., 1996, "Lecture notes for the course Fuzzy decision making", Department of operations research, Eotvos Lorand university. http//www.abo.fi/~rfuller/fdm.html

Gill R. S., Nielsen P. and Valeur H. H.: Evaluation of the ERS.SAR high resolution precision images in the operational mapping of sea ice in the Kap Farvel waters , Proceedings of the Second ERS Application workshop, London 6th. - 8th. , 1995.

Gill R. S. and Valeur H. H. (1999). "Ice cover discrimination in the Greenland waters using first-order texture parameters of ERS SAR images", Int. J. Remote Sensing, vol. 20, no. 2, pp. 373 - 385.

Gill R. S., Rosengreen M. K: and Valeur H. H. (2000). "Operational Ice Mapping with RADARSAT for ship navigation in the Greenlandic Waters", Canadian Journal of Remote Sensing, vol. 26, No. 2, pp. 121 - 132.

Gill R. S., (2001). "Sea Ice Edge and Icebergs Detection using routine operations". Canadian J. REMOTE SENSING, special issue on Sea Ice and Icebergs, ivol. 27, no. 5, pp 411 – 432.

Gill R. S., 2002, "SAR surface classification using distribution matching", DANISH MET. SCIENTIFIC REPORT, 02 -08.

Haverkamp D. and Tsatsoulis C., 1999, "Information Fusion for estimation of Summer MIZ Ice Concentration for SAR Imagery", IEEE Trans. Geoscience and Remote Sensing, vol. 37, no. 3, page 1278.

Haverkamp D. and Tsatsoulis C., 1995, "A comprehensive, Automated Apporach to Determining Sea Ice Thickness from SAR data", ", IEEE Trans. Geoscience and Remote Sensing, vol. 33, no. 1, page 46.

Kohonen, T., Hynninen, J., Kangas, J., Laaksonen, J., and Torkkola, K., 1995, "LVQ-PAK: the learning vector quanitsation program package, version 3.1. technical Report, Laboratory of Computer and Information Science, Helsinki University of technology, Finland.

Leen-Kait Soh, Haverkamp D. and Tsatsoulis C., 199?, "Separating Ice – water Composites and Computing Floe Size Distributions", ….. where published ?
Korsnes R., 1993, "Quantitative analysis of sea ice remote sensing imagery", INT. J. REMOTE SENSING, vol. 14, no. 2, 295 – 311.

Masselli F., Conese C., Filippis F. D., and Norcini S. 1995, "Estimation of Forest Parameters Trough Fuzzy Classification of TM Data", IEEE Trans. Geoscience and Remote Sensing, vol. 33, no. 1, page 77.

Melgani F., Bakir A. r. Al Hasheny, and Taha S. M. R., 2000, "An Explicit Fuzzy Supervised Classification Method for Multispectral Remote Sensing Images", IEEE Trans. Geoscience and Remote Sensing, vol. 38, no. 1, page 287.

Moore T. S., Campbell J. W., and Feng H., 2001, "AFuzzy Logic Classification Scheme for Selecting and Blending Satellite Ocean Colour Algorithms", IEEE Trans. Geoscience and Remote Sensing, vol. 39, no. 8, page 1764.

Pal S. K., Ghosh A., Shankar B. U., 2000, "Segmentation of Remotely Sensed Images with Fuzzy Thresholding and Quantitative Evaluation", INT. J. REMOTE SENSING, vol. 21, no 11, 2269 – 2300.

Solaiman B., Pierce L. E., and Ulaby F. T., 1999, "Multisensor Data Fusion Using Fuzzy Concepts: Application to Land – Cover Classification Using ERS-1/JERS-1 SAR Composites", IEEE Trans. Geoscience and Remote Sensing, vol. 37, no. 3, page 1316.

Tupin F., Bloch I., and Maitre H., 1999, "A First Step Toward Automatic Interpretation of SAR Images Using Evidential Fusion of Several Structure Detectors", IEEE Trans. Geoscience and Remote Sensing, vol. 37, no. 3, page 1327.

Wu D and Linders J., 2000, "Camparison of three different methods to select feature for discriminating forest cover types using SAR imagery", INT. J. REMOTE SENSING, vol. 10, no. 10, 2089 – 2099.

Yager R. R., 1993, "Fuzzy Screening Systems", in R. Lowen and M. Roubens eds., Fuzzy Logic: State of the Art (Kluwer, Dordrecht), pp. 251 – 261.

Zadeh L. A., 1965, "Fuzzy sets", Inform. Contr. Vol. 8, pp. 338 – 353.

Zhang J., and Foody G. M., 2001, "Fully-fuzzy supervised classification of sub-urban land cover from remotely sensed imagery: statistical and artificial neutral network approaches", INT. J. REMOTE SENSING, vol. 22, no 4, 615 – 628.

7. Figures
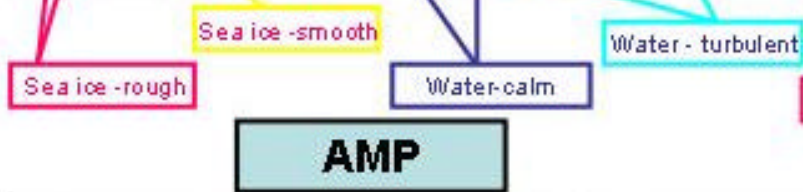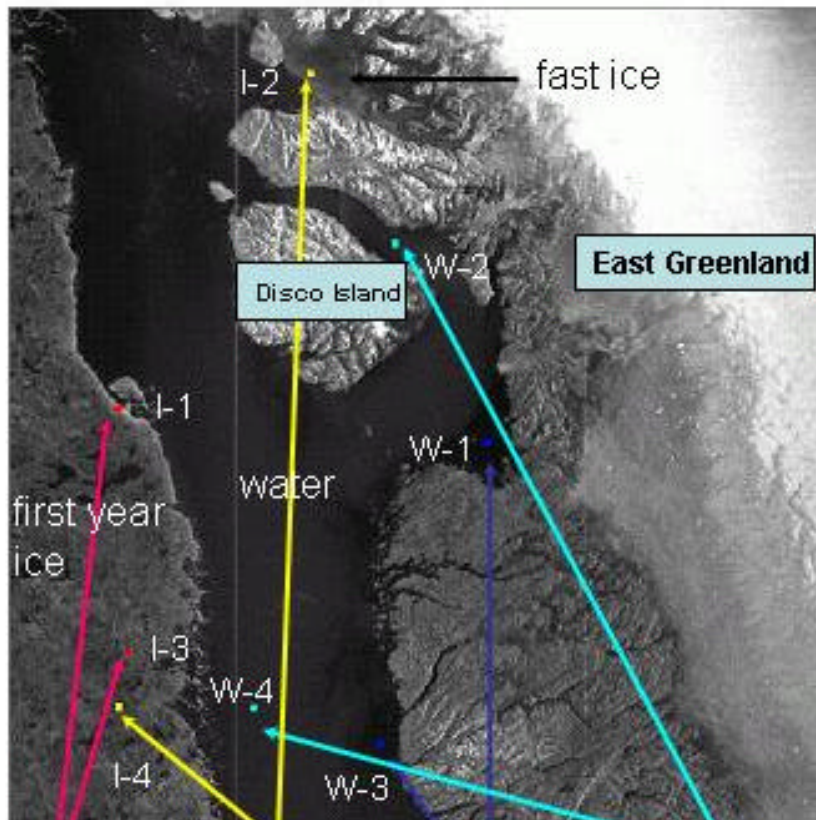
Figure 2. 4*4 pixel averaged RADARSAT *AMPLITUDE* image from West Greenland from 2000-05-24. The swath length, from left to right is 500 km.
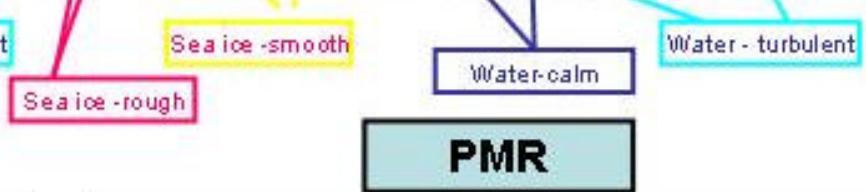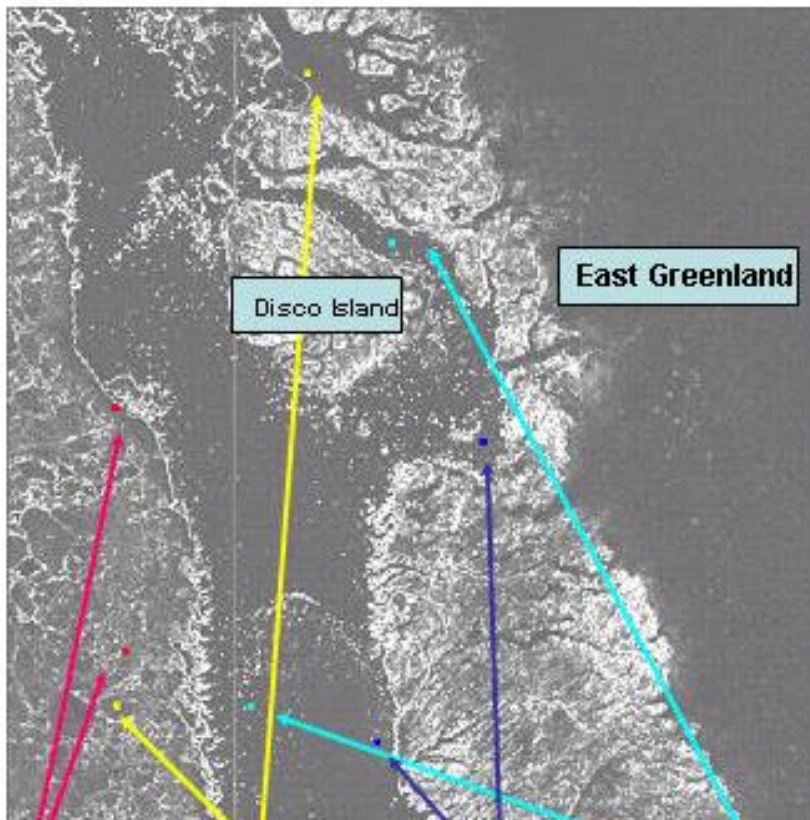
Figure 3. *PMR product* corresponding to fig.2 on the left shown on a grey level scale. PMR values have been multiplied by a factor of 100.
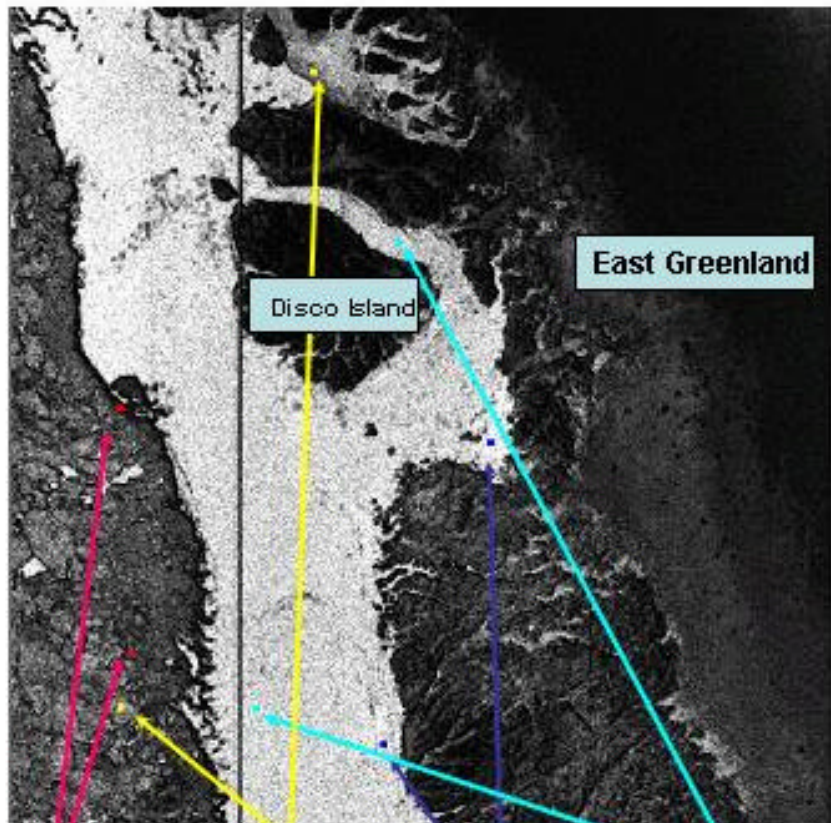
Figure 4. *GAMMA product* corresponding to fig.2 above shown on a grey level scale. Gamma probabilities have been multiplied by a factor of 10^5.
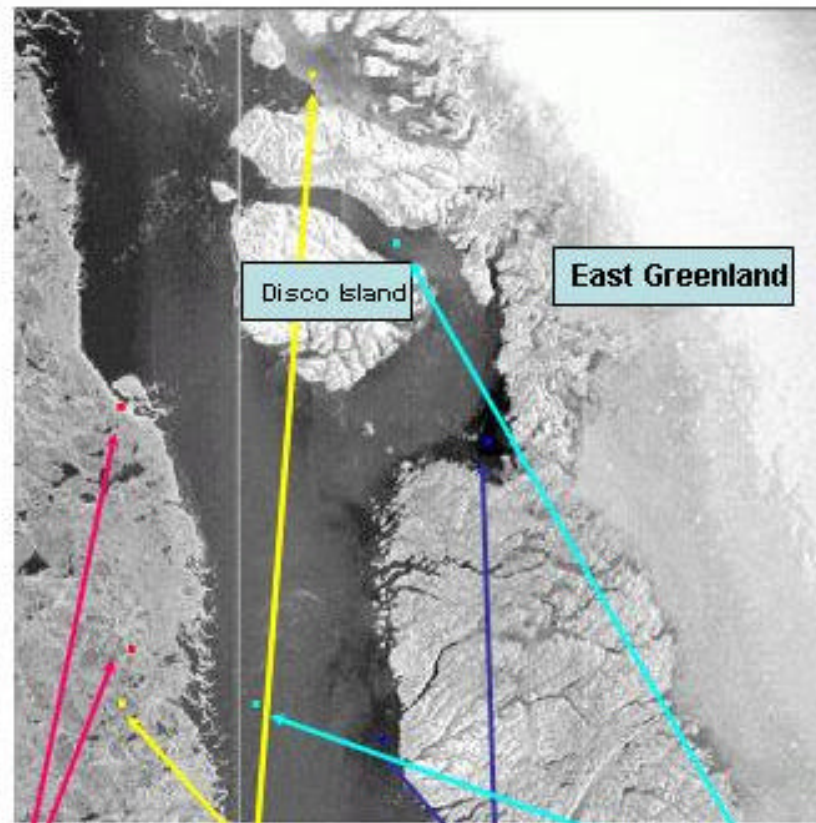
Figure 5. *ENTROPY product* corresponding to fig.2 above shown on a grey level scale. ENT values have been multiplied by a factor of 40.

ice misclassified as water

East Greenland

Disco Island
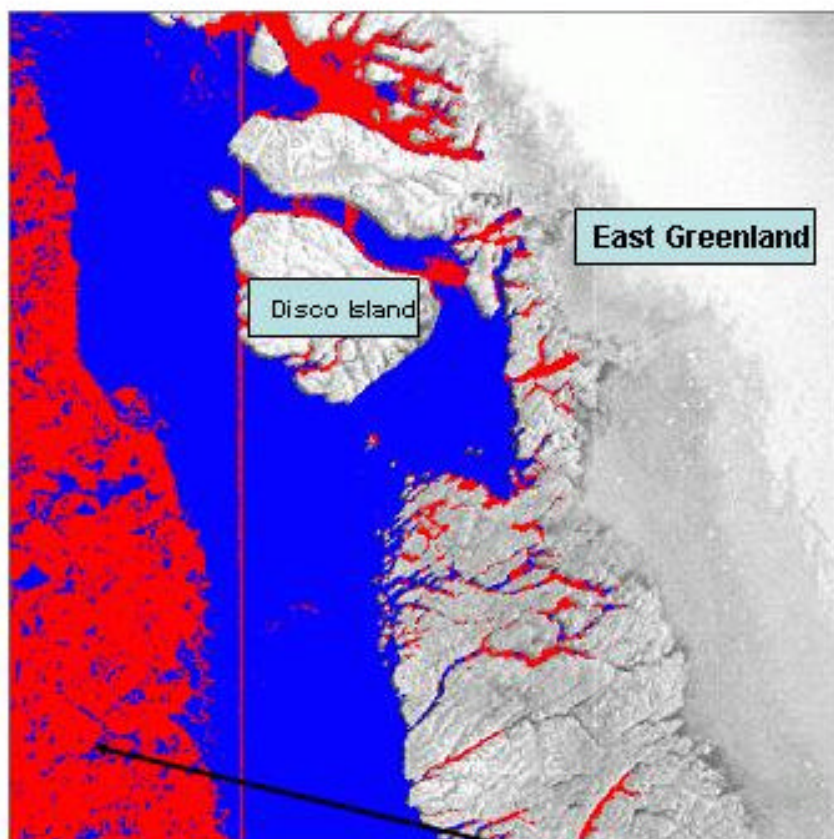
ice regions misclassified as water

Fig. 6. Classification of the RADARSAT image shown in fig. 2 using only (i) *KS criterion*, (ii) 2 pre-defined classes (water: W-4 and ice: I-3 shown in fig.2), and (iii) *AMP expert*.
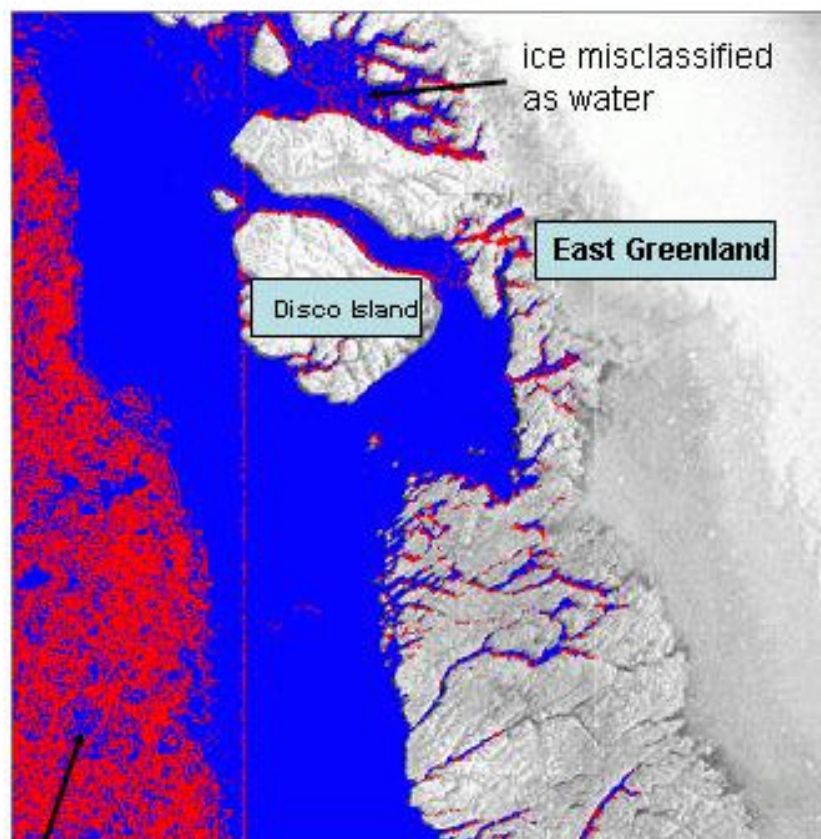
**Fig. 7.** Classification of the RADARSAT image shown in fig. 2 using only (i) *KS criterion*, (ii) 2 pre-defined classes (water: W-4 and ice: I-3 shown in fig.2), and (iii) *AMP and PMR experts.*

Colour code: ■ = sea ice, ■ = water

ice misclassified
as water

East Greenland

Disco Island

East Greenland

Disco Island

ice regions misclassified as water
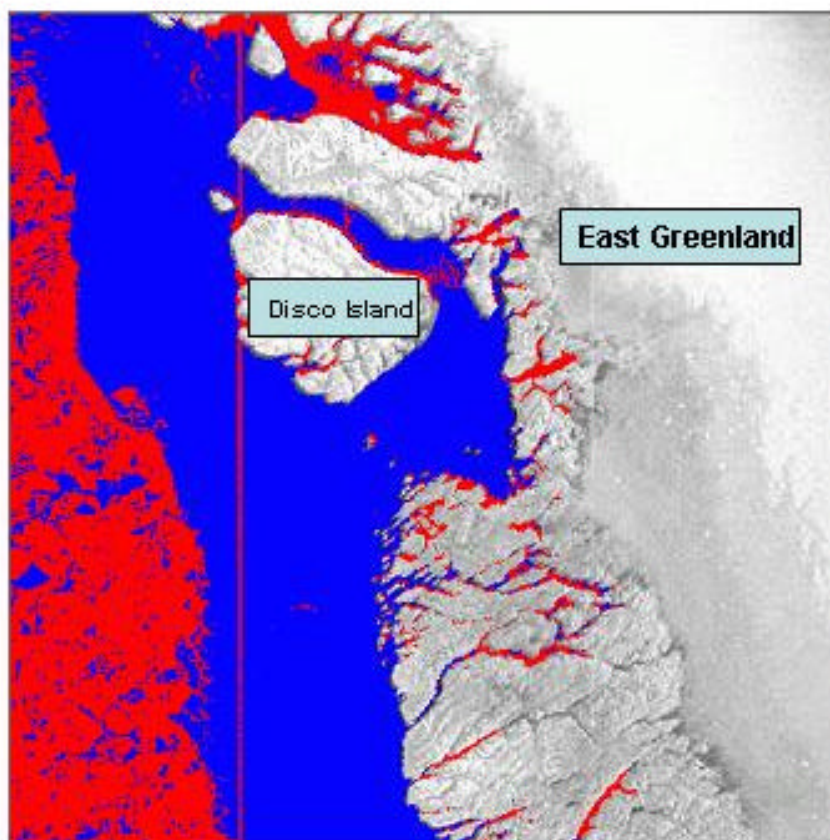
Fig. 8. Classification of the RADARSAT image shown in fig. 2 using only (i) *KS criterion*, (ii) 2 pre-defined classes (water: W-4 and ice: I-3 shown in fig.2), and (iii) *AMP and GAMMA experts*.
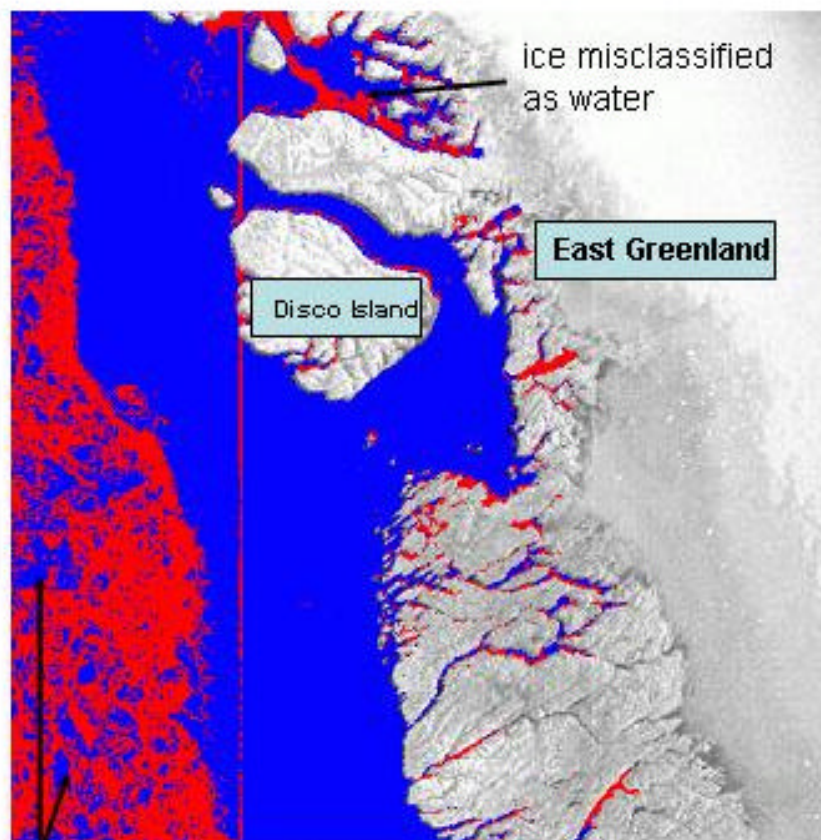
Fig. 9. Classification of the RADARSAT image shown in fig. 2 using only (i) *KS criterion*, (ii) 2 pre-defined classes (water: W-4 and ice: I-3 shown in fig.2), and (iii) *AMP and ENT experts*.

Colour code: ■ = sea ice, ■ = water

ice misclassified as water
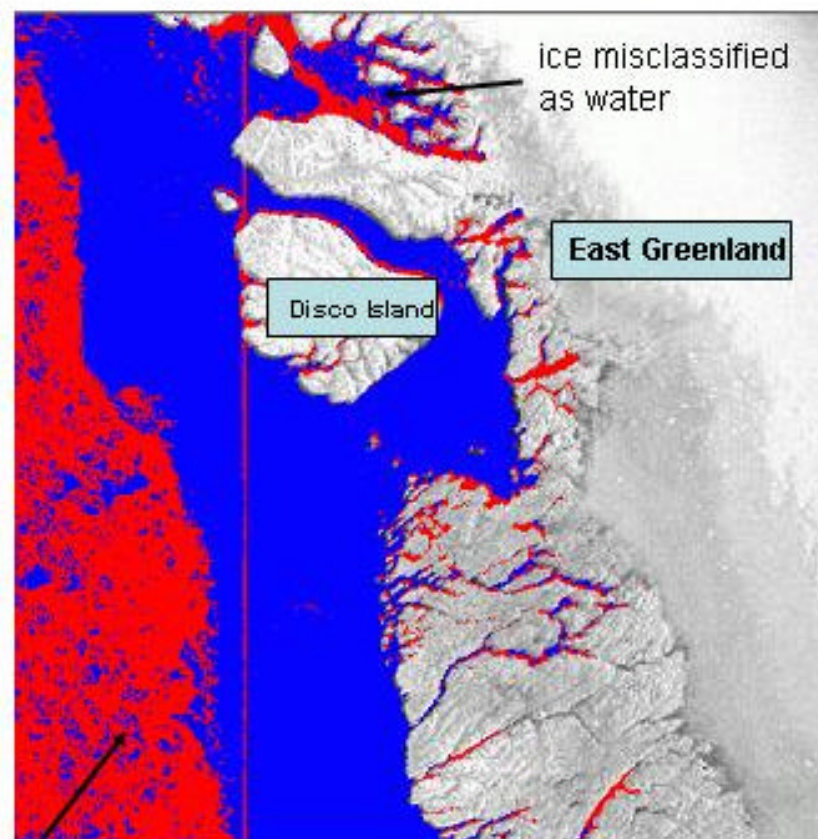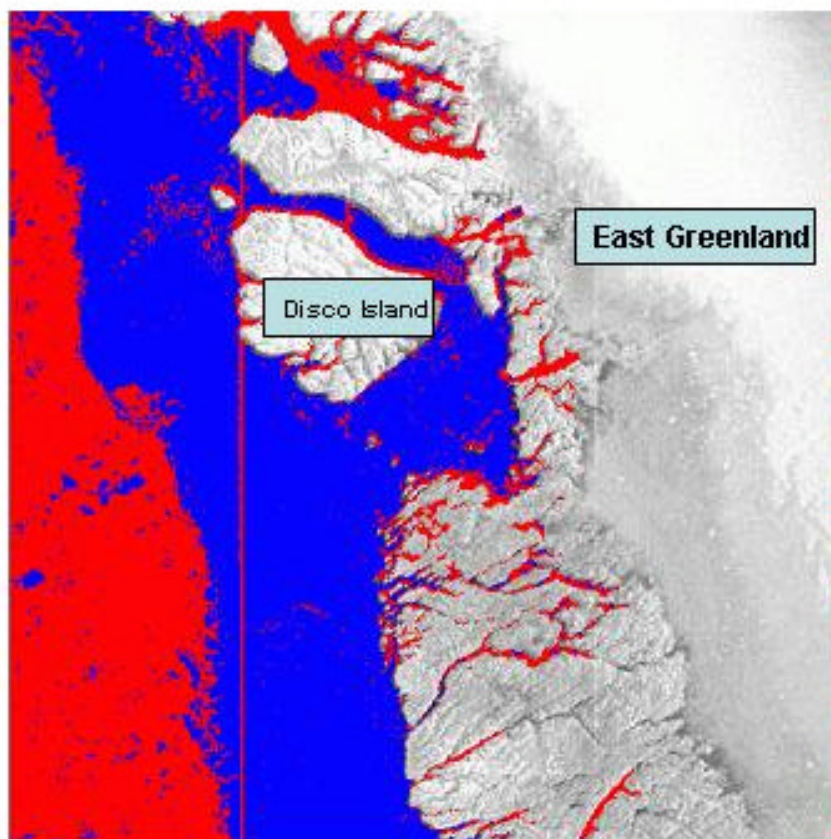
ice regions misclassified as water

Fig. 10. Classification of the RADARSAT image shown in fig. 2 using only (i) **KS criterion**, (ii) 2 pre-defined classes (water: W-4 and ice: I-3 shown in fig.2), and (iii) **AMP, PMR and GAMMA experts.**

**Fig. 11.** Classification of the RADARSAT image shown in fig. 2 using only (i) **KS criterion**, (ii) 2 pre-defined classes (water: W-4 and ice: I-3 shown in fig.2), and (iii) **AMP, PMR, GAMMA and ENT experts.**

Colour code: ■ = sea ice, ■ = water

ice misclassified as water

ice regions misclassified as water
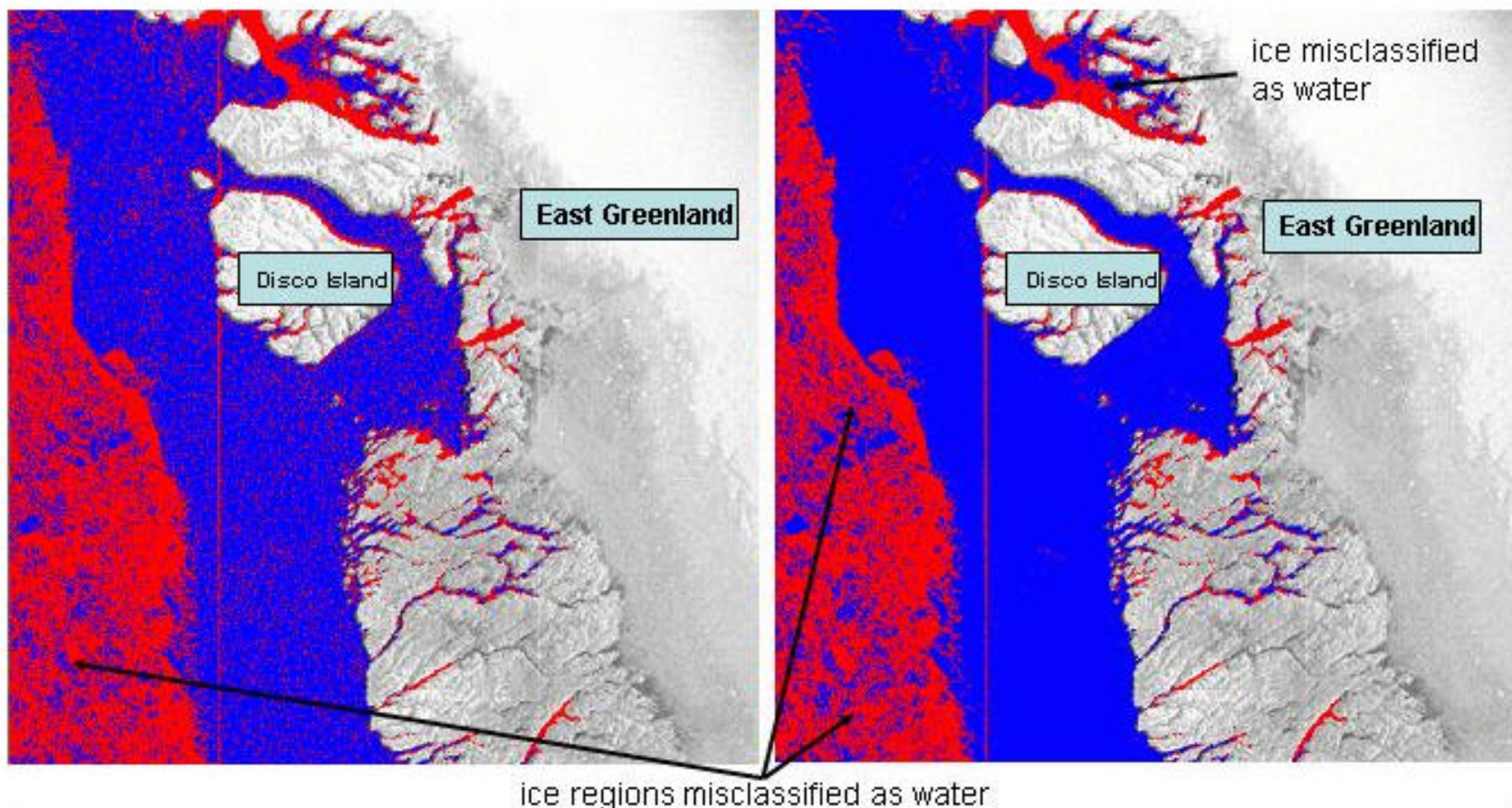
Fig. 12. Classification of the RADARSAT image shown in fig. 2 using only (i) *mean values criterion*, (ii) 2 pre-defined classes (water: W-4 and ice: I-3 shown in fig.2), and (iii) *AMP, PMR and GAMMA experts.*

Fig. 13. Classification of the RADARSAT image shown in fig. 2 using only (i) *mean values criterion*, (ii) 2 pre-defined classes (water: W-4 and ice: I-3 shown in fig.2), and (iii) *AMP, PMR, GAMMA and ENT experts.*

Colour code: ■ = sea ice, ■ = water

ice misclassified as water

East Greenland

Disco Island
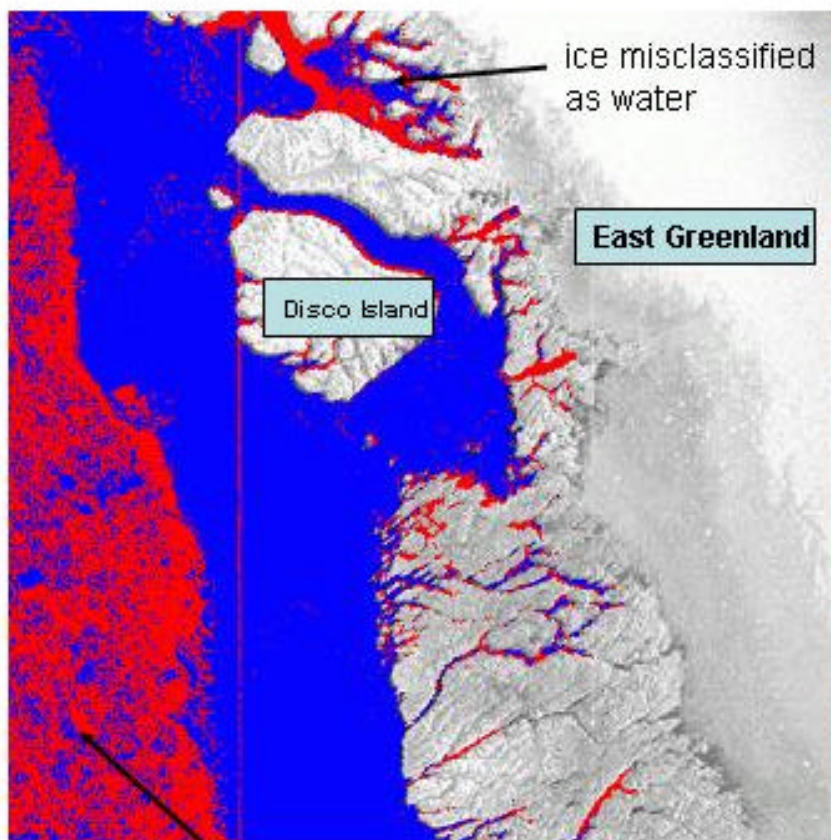
ice regions misclassified as water

Fig. 14. Classification of the RADARSAT image shown in fig. 2 using (i) KS and mean values criteria with *equal importance to both*, (ii) 2 pre-defined classes (water: W-4 and ice: I-3 shown in fig.2), and (iii) *AMP, PMR and GAMMA experts.*

Fig. 15. Classification of the RADARSAT image shown in fig. 2 using (i) KS and mean values criteria with *less importance to mean values*, (ii) 2 pre-defined classes (water: W-4 and ice: I-3 shown in fig.2), and (iii) *AMP, PMR and GAMMA experts.*

Colour code: ■ = sea ice, ■ = water

ice misclassified as water

East Greenland

Disco Island
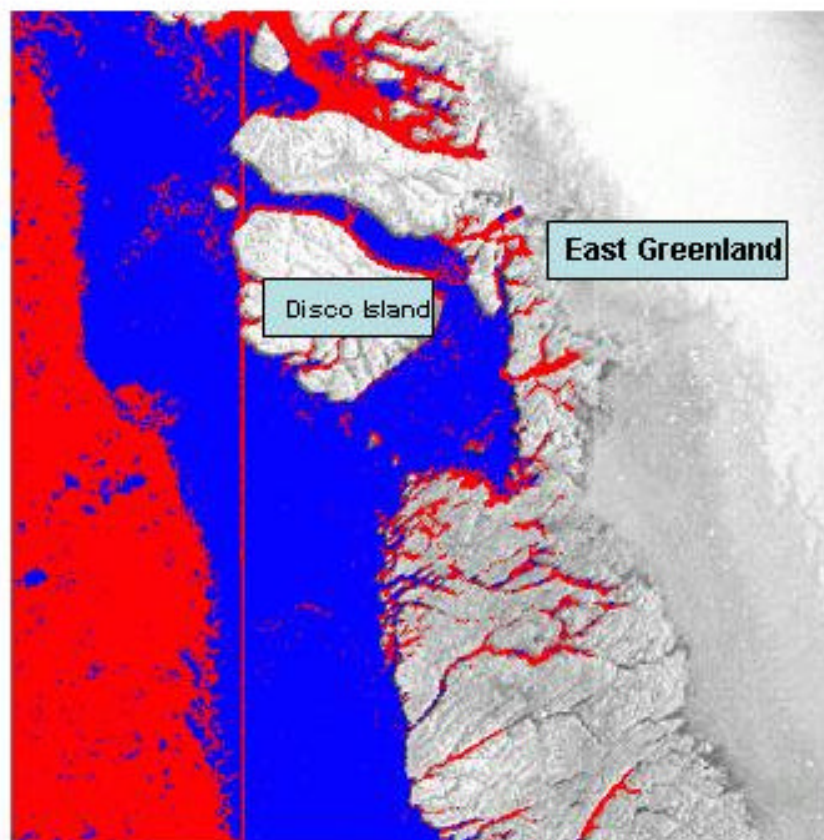
ice regions misclassified as water
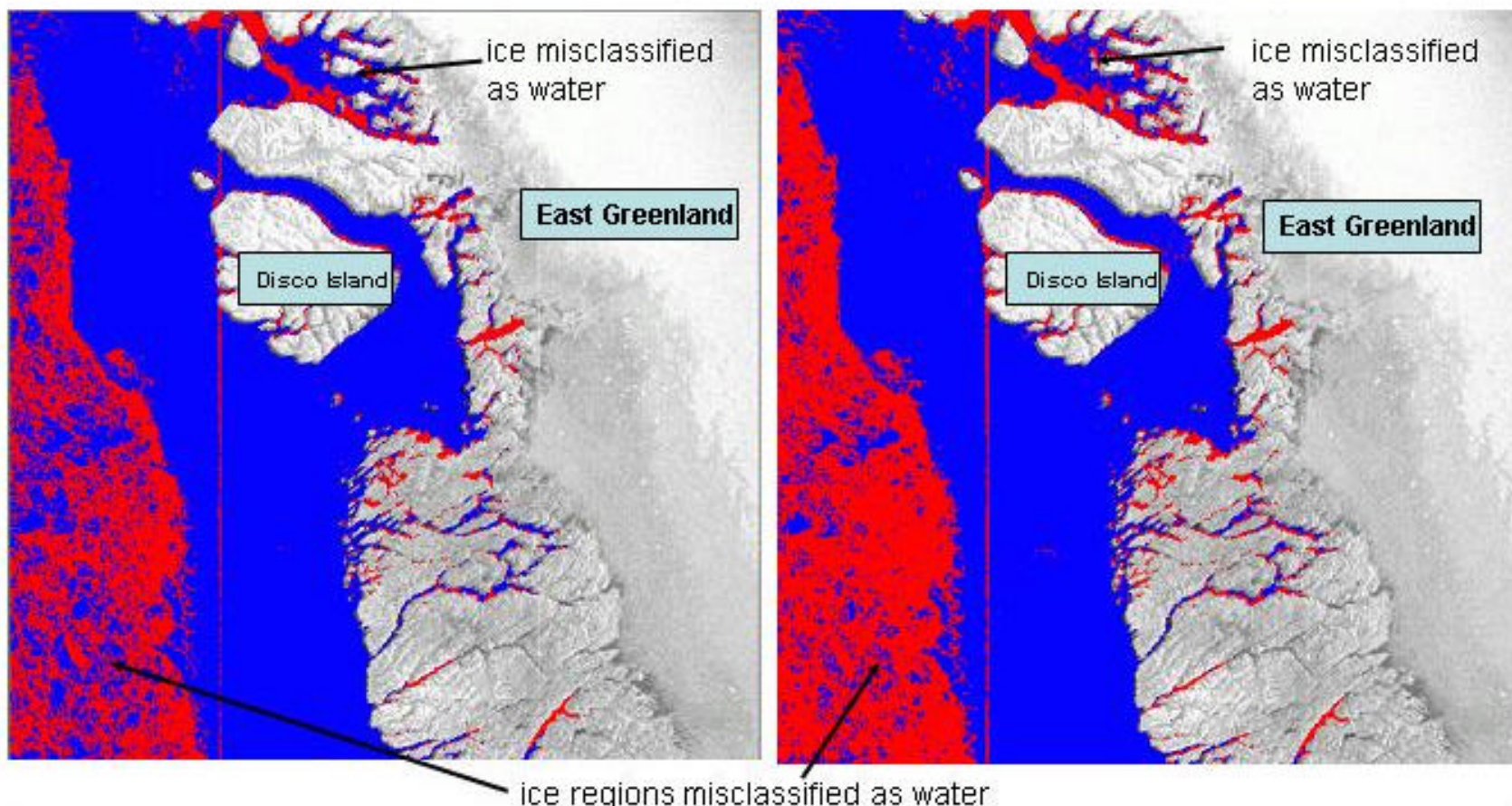
Fig. 16. Classification of the RADARSAT image shown in fig. 2 using (i) KS and mean values criteria with *equal importance to both*, (ii) 2 pre-defined classes (water: W-4 and ice: I-3 shown in fig.2), and (iii) *AMP, PMR, GAMMA and ENT experts.*

Fig. 17. Classification of the RADARSAT image shown in fig. 2 using (i) KS and mean values criteria with *less importance to mean values*, (ii) 2 pre-defined classes (water: W-4 and ice: I-3 shown in fig.2), and (iii) *AMP, PMR, GAMMA and ENT experts.*

Colour code: ▉ = sea ice, ▉ = water
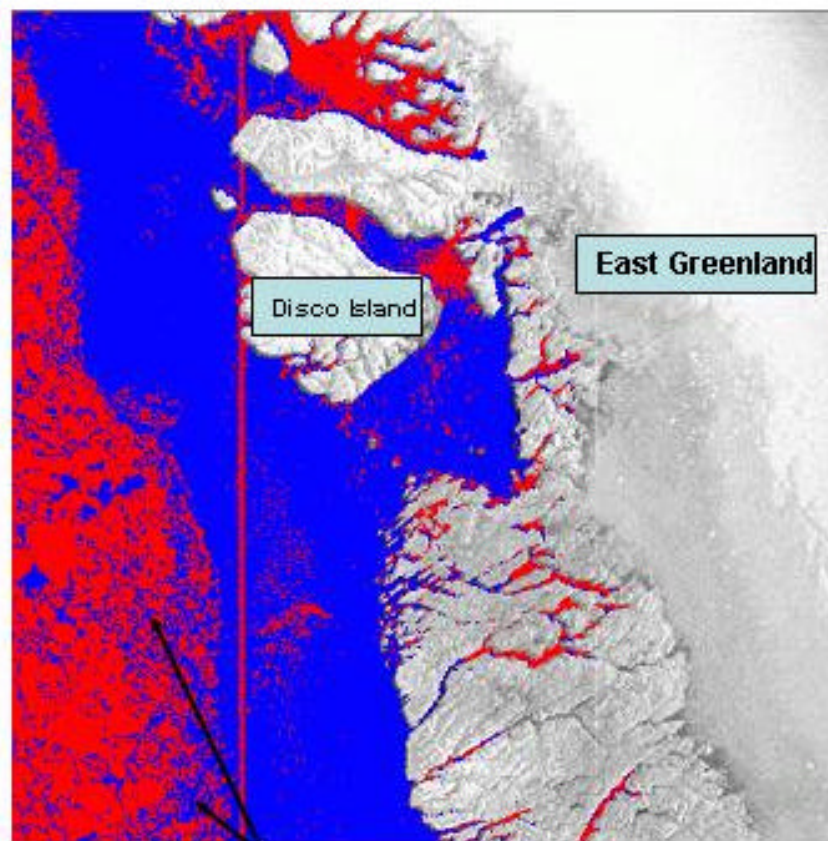
ice regions misclassified as water

Fig. 18. Classification of the RADARSAT image shown in fig. 2 using (i) KS and mean values criteria with less importance to mean values, (ii) 2 pre-defined classes (*water: W-3 and ice: I-4* shown in fig.2), and (iii) *AMP, PMR, GAMMA and ENT experts.*

Colour code: ■ = sea ice, ■ = water
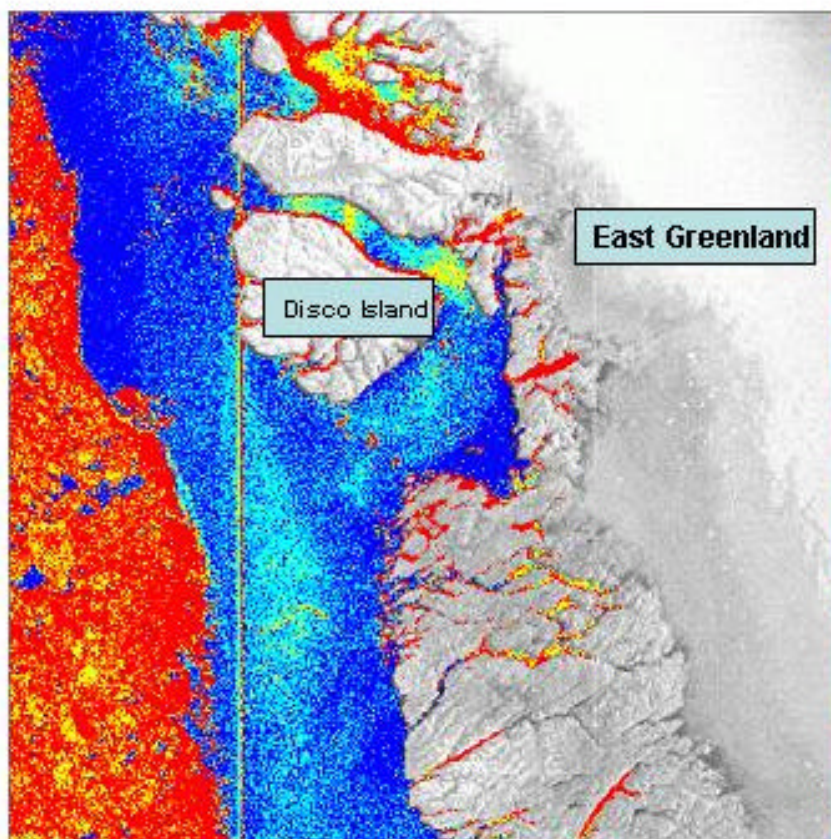
Fig. 19. Classification of the RADARSAT image shown in fig. 2 using (i) KS and mean values criteria with less importance to mean values, (ii) *4 pre-defined classes (water: W-3 and W-4, ice: I-3 and I-4* shown in fig.2), and (iii) *AMP, PMR and GAMMA experts.*
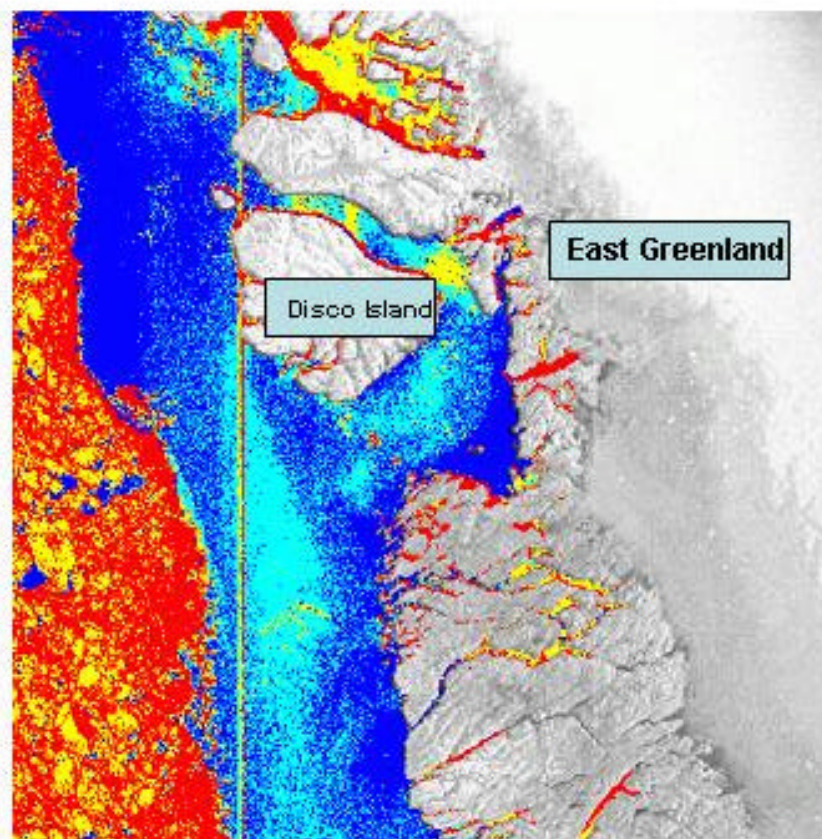
Fig. 20. Classification of the RADARSAT image shown in fig. 2 using (i) KS and mean values criteria with less importance to mean values, (ii) *4 pre-defined classes (water: W-3 and W-4, ice: I-3 and I-4* shown in fig.2), and (iii) *AMP, PMR, GAMMA and ENT experts.*
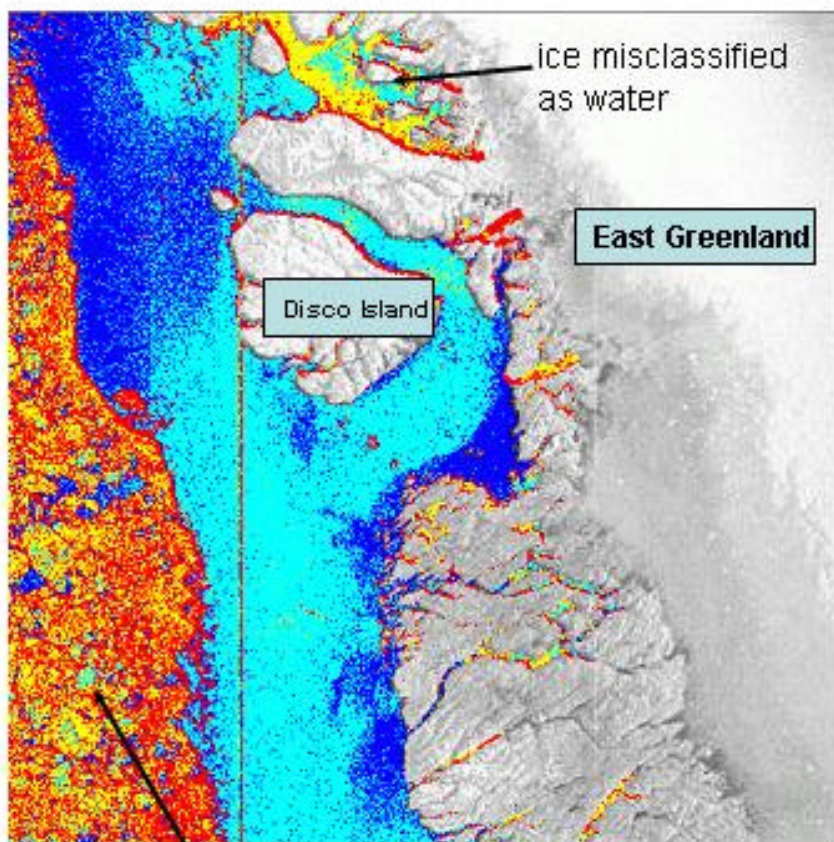
Colour code: ■ = ice low backscatter, □ = ice high backscatter, ■ =calm water, □ =turbulent water

Fig. 21. Classification of the RADARSAT image shown in fig. 2 using (i) KS and mean values criteria with less importance to mean values, (ii) *8 pre-defined classes (4 classes of water and ice each*, shown in fig.2), and (iii) *AMP, PMR and GAMMA experts.*
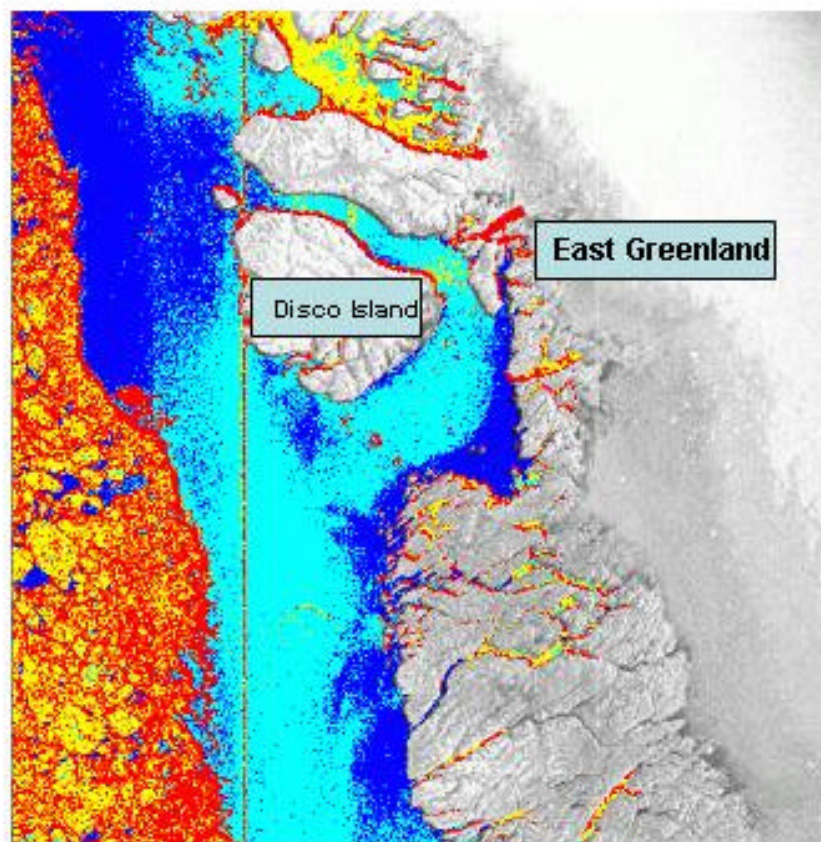
Fig. 22. Classification of the RADARSAT image shown in fig. 2 using (i) KS and mean values criteria with less importance to mean values, (ii) *8 pre-defined classes (4 classes of water and ice* shown in fig.2), and (iii) *AMP, PMR, GAMMA and ENT experts.*

Colour code: ■ = ice low backscatter, ■ = ice high backscatter, ■ =calm water, ■ =turbulent water
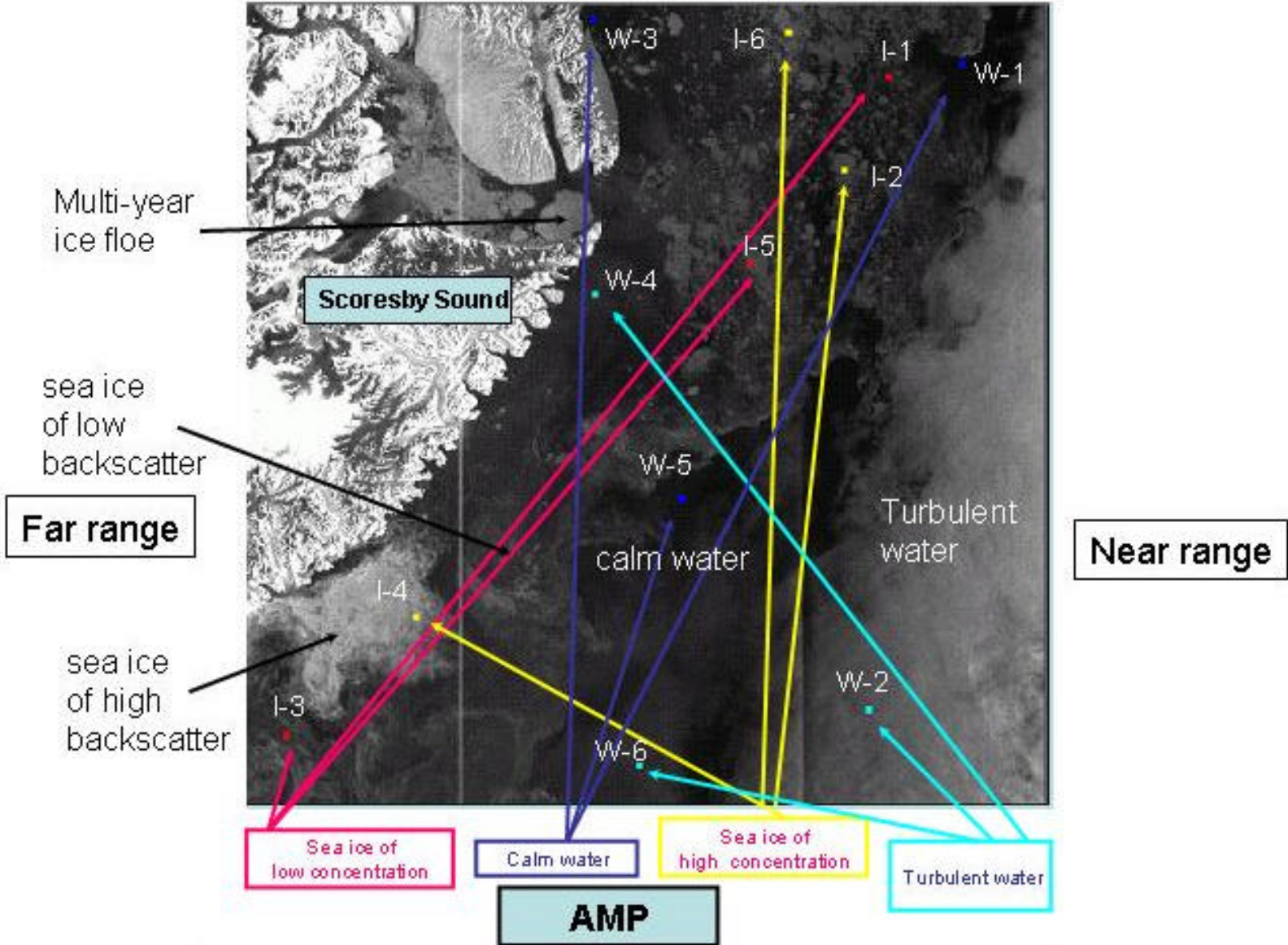
**Figure 23.** 4*4 pixel averaged RADARSAT *AMPLITUDE* image from East Greenland from 2000-07-22. The swath is 500 km.
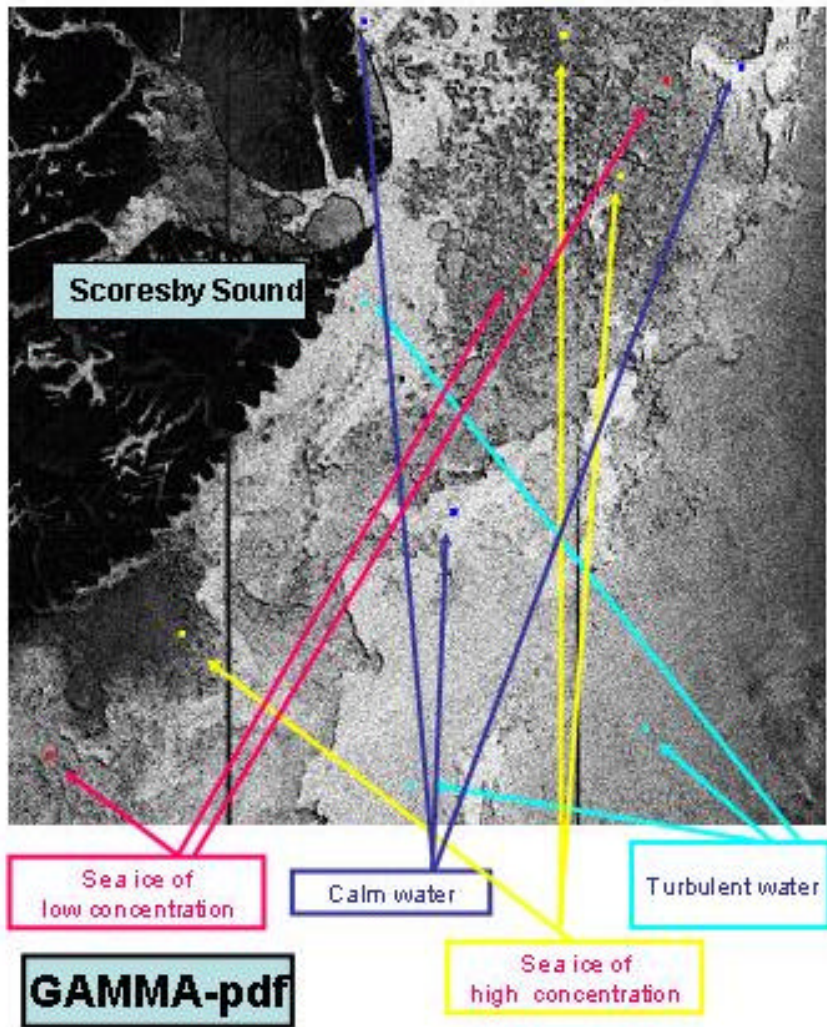
Figure 24. *GAMMA product* corresponding to fig.23 above shown on a grey level scale. Gamma probabilities have been multiplied by a factor of 10^5.
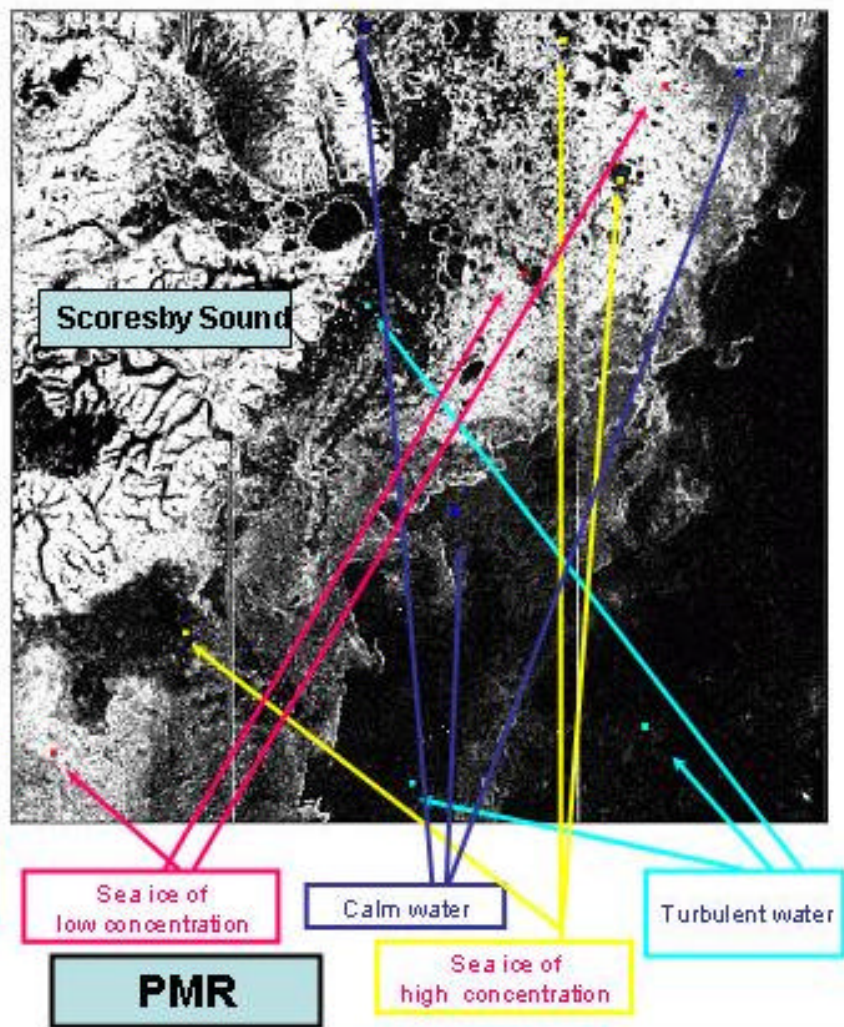
Figure 25. *PMR product* corresponding to fig.23 shown above on a grey level scale. PMR values have been multiplied by a factor of 100.

ice misclassified as water   water misclassified as ice
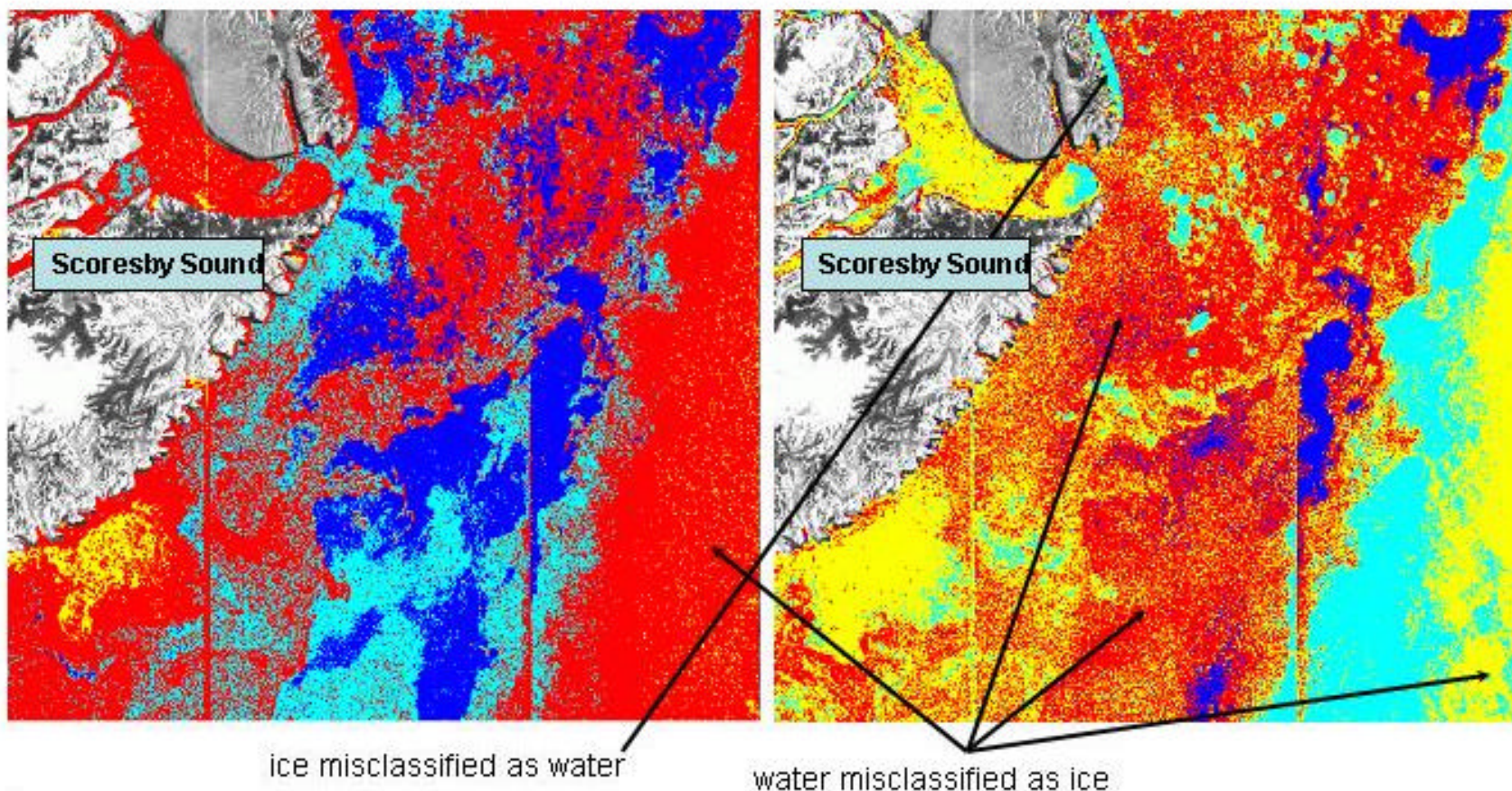
Fig. 26. Classification of the RADARSAT image shown in fig. 23 using (i) KS and mean values criteria with less importance to mean values, (ii) *4 pre-defined classes in the far range (water: W-3 and W-4, Ice:I-3 and I-4,* shown in fig.23), and (iii) *AMP, PMR and GAMMA experts.*

Fig. 27. Classification of the RADARSAT image shown in fig. 23 using (i) KS and mean values criteria with less importance to mean values, (ii) *4 pre-defined classes in the near range (water: W-1 and W-2, Ice:I-1 and I-2,* shown in fig.23), and (iii) *AMP, PMR and GAMMA experts.*

Colour code: ■ = ice low backscatter, ■ = ice high backscatter, ■ =calm water, ■ =turbulent water

40

Scoresby Sound
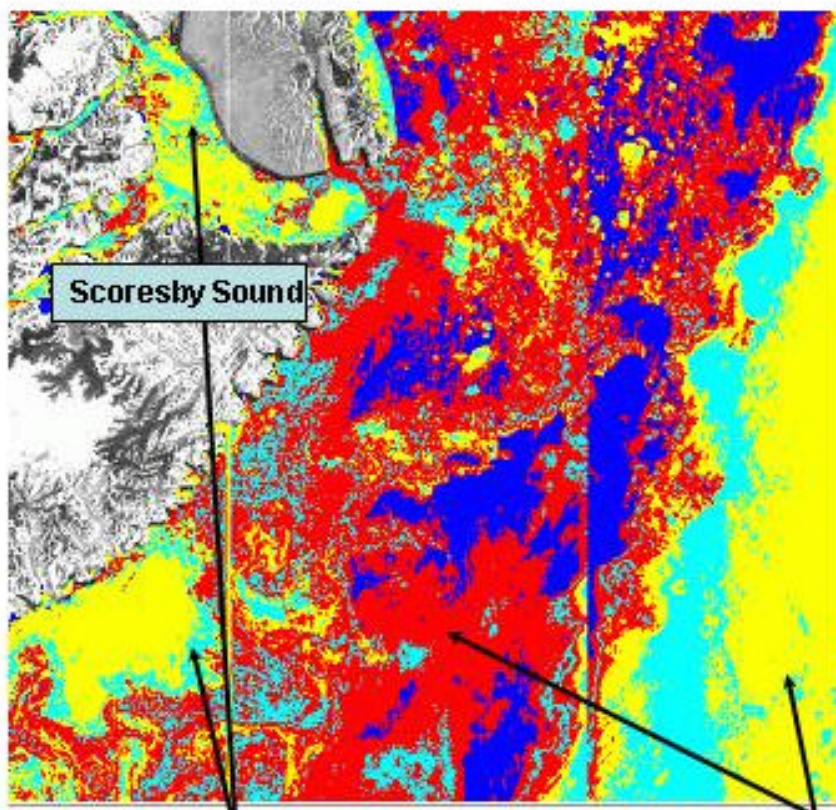
ice misclassified as water

water misclassified as ice

XX

Fig. 28. Classification of the RADARSAT image shown in fig. 23 using only (i) KS criterion, (ii) *8 pre-defined classes (water: W-1 to W-4 and ice: I-1 to I-4*, shown in fig.23), and (iii) *AMP expert.*

Fig. 29. Classification of the RADARSAT image shown in fig. 23 using only (i) KS criterion, (ii) *8 pre-defined classes (water: W-1 to W-4 and ice: I-1 to I-4,* shown in fig.23), and (iii) *AMP and GAMMA experts.*

Colour code: ▮ = ice low backscatter, ▯ = ice high backscatter, ▮ =calm water, ▯ =turbulent water

water misclassified as ice
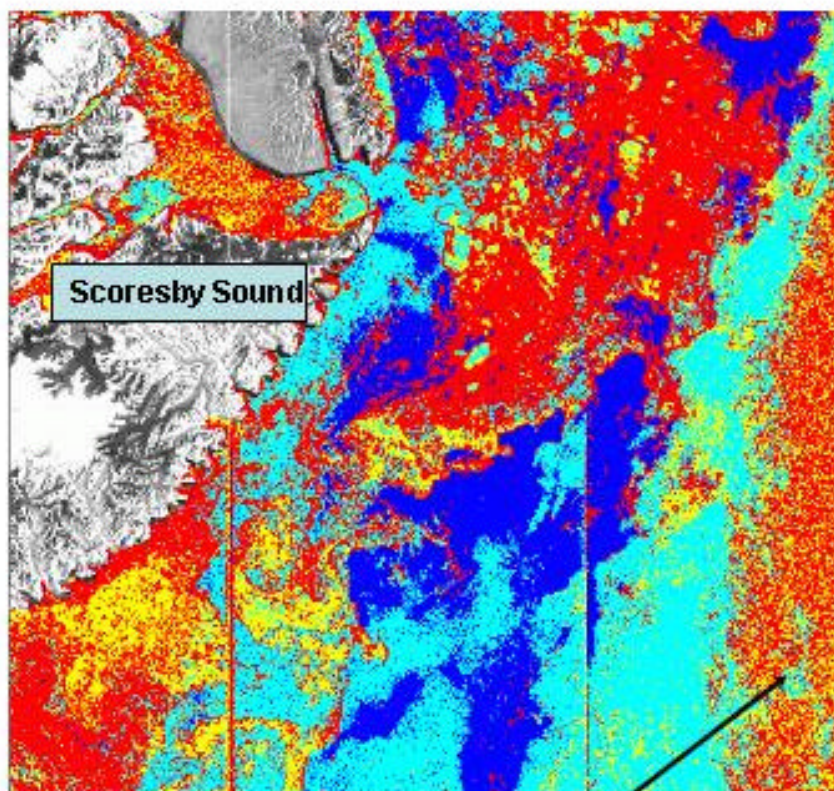
Ice misclassified as water

Fig. 30. Classification of the RADARSAT image shown in fig. 23 using only (i) *KS criterion*, (ii) *8 pre-defined classes (water: W-1 to W-4 and ice: I-1 to I-4*, shown in fig.23), and (iii) *AMP, GAMMA and PMR experts.*
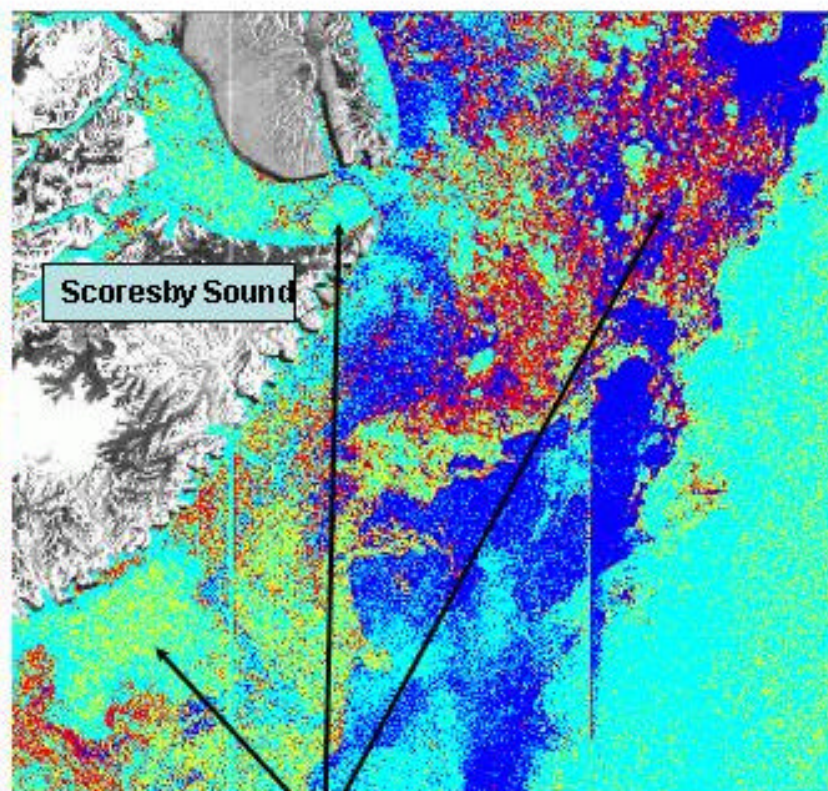
Fig. 31. Classification of the RADARSAT image shown in fig. 23 using only (i) *mean values criterion*, (ii) *8 pre-defined classes (water: W-1 to W-4 and ice: I-1 to I-4*, shown in fig.23), and (iii) *AMP, GAMMA, PMR experts.*

Colour code: ■ = ice low backscatter, ■ = ice high backscatter, ■ =calm water, ■ =turbulent water
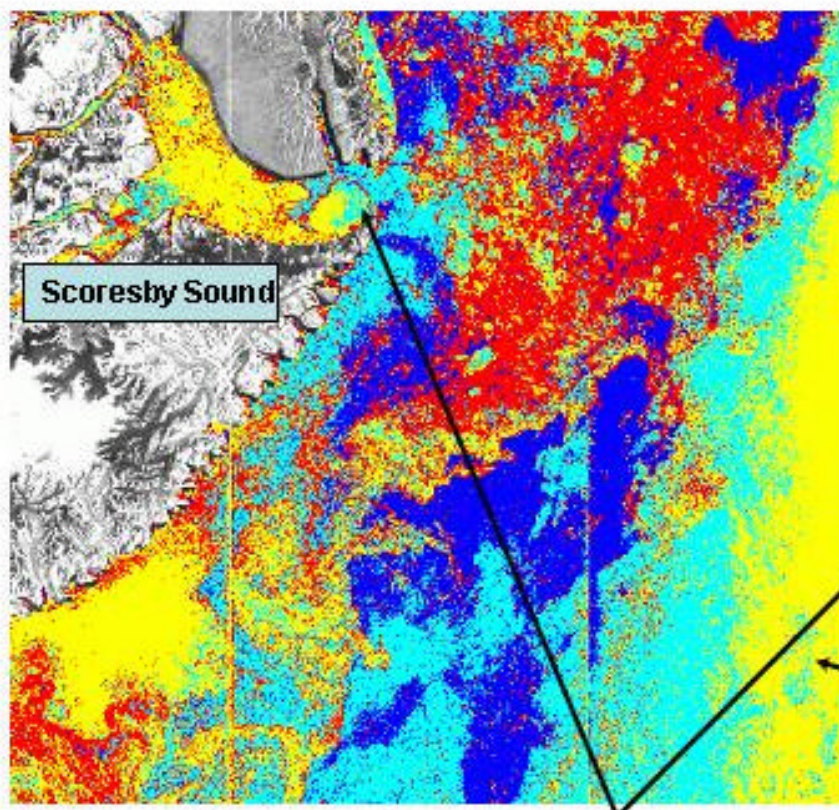
ice misclassified as water

water misclassified as ice

Fig. 32. Classification of the RADARSAT image shown in fig. 23 using (i) *KS and mean values Criteria with less importance to mean values*, (ii) *8 pre-defined classes (water: W-1 to W-4 and ice: I-1 to I-4,* shown in fig.23), and (iii) *AMP, GAMMA and PMR experts.*
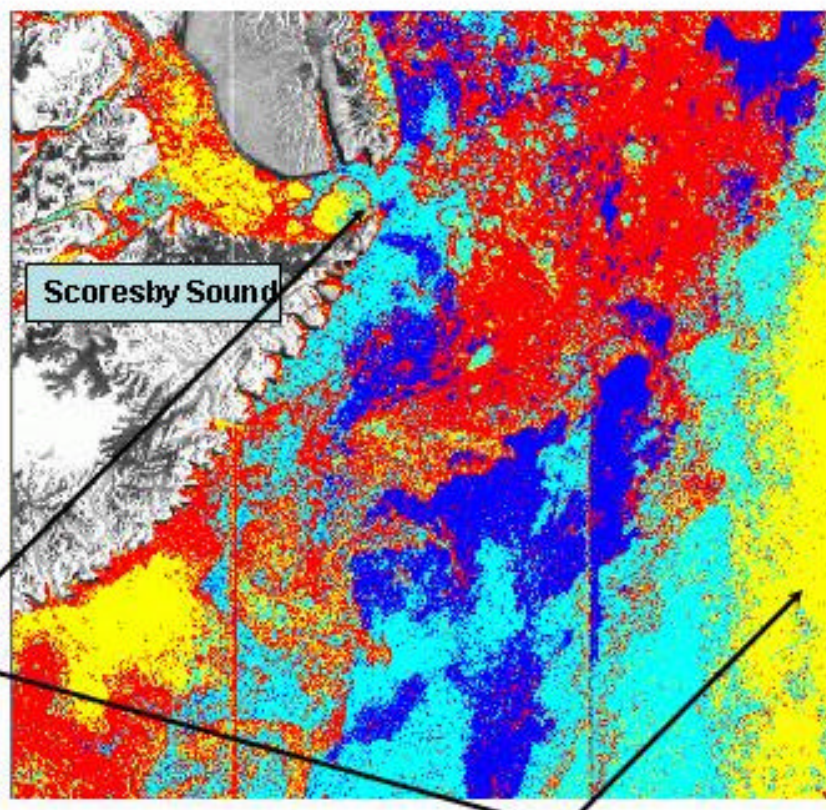
Fig. 33. Classification of the RADARSAT image shown in fig. 23 using (i) *KS and mean values Criteria with less importance to mean values*, (ii) *12 pre-defined classes (water: W-1 to W-6 and ice: I-1 to I-6,* shown in fig.23), and (iii) *AMP, GAMMA and PMR experts.*

Colour code: ■ = ice low backscatter, ■ = ice high backscatter, ■ =calm water, ■ =turbulent water

8. Danish Meteorological Institute - Scientific Reports

Scientific reports from the Danish Meteorological Institute cover a variety of geo physical fields, i.e. meteorology (including climatology), oceanography, subjects on air and sea pollution, geomagnetism, solar-terrestrial physics, and physics of the middle and upper atmosphere.

Reports in the series within the last five years:

No. 97-1
E. Friis Christensen og C. Skøtt: Contributions from the International Science Team. The Ørsted Mission - a pre-launch compendium

No. 97-2
Alix Rasmussen, Sissi Kiilsholm, Jens Havskov Sørensen, Ib Steen Mikkelsen: Analysis of tropospheric ozone measurements in Greenland: Contract No. EV5V-CT93-0318 (DG 12 DTEE): DMI's contribution to CEC Final Report Arctic Trophospheric Ozone Chemistry ARCTOC

No. 97-3
Peter Thejll: A search for effects of external events on terrestrial atmospheric pressure: cosmic rays

No. 97-4
Peter Thejll: A search for effects of external events on terrestrial atmospheric pressure: sector boundary crossings

No. 97-5
Knud Lassen: Twentieth century retreat of sea-ice in the Greenland Sea

No. 98-1
Niels Woetman Nielsen, Bjarne Amstrup, Jess U. Jørgensen: HIRLAM 2.5 parallel tests at DMI: sensitivity to type of schemes for turbulence, moist processes and advection

No. 98-2
Per Høeg, Georg Bergeton Larsen, Hans-Henrik Benzon, Stig Syndergaard, Mette Dahl Mortensen: The GPSOS project. Algorithm functional design and analysis of ionosphere, stratosphere and troposphere observations

No. 98-3
Mette Dahl Mortensen, Per Høeg:
Satellite atmosphere profiling retrieval in a nonlinear troposphere. Previously entitled: Limitations induced by Multipath

No. 98-4
Mette Dahl Mortensen, Per Høeg: Resolution properties in atmospheric profiling with GPS

No. 98-5
R.S. Gill and M. K. Rosengren: Evaluation of the Radarsat imagery for the operational mapping of sea ice around Greenland in 1997

No. 98-6
R.S. Gill, H.H. Valeur, P. Nielsen and K.Q. Hansen: Using ERS SAR images in the operational mapping of sea ice in the Greenland waters: final report for ESA-ESRIN's: pilot projekt no. PP2.PP2.DK2 and 2nd announcement of opportunity for the exploitation of ERS data projekt No. AO2..DK 102

No. 98-7
Per Høeg et al.: GPS Atmosphere profiling methods and error assessments

No. 98-8
H. Svensmark, N. Woetmann Nielsen and A.M. Sempreviva: Large scale soft and hard turbulent states of the atmosphere

No. 98-9
Philippe Lopez, Eigil Kaas and Annette Guldberg: The full particle-in-cell advection scheme in spherical geometry

No. 98-10
H. Svensmark: Influence of cosmic rays on earth's climate

No. 98-11
Peter Thejll and Henrik Svensmark: Notes on the method of normalized multivariate regression

No. 98-12
K. Lassen: Extent of sea ice in the Greenland Sea 1877-1997: an extension of DMI Scientific Report 97-5

No. 98-13
Niels Larsen, Alberto Adriani and Guido DiDon-francesco: Microphysical analysis of polar strato-spheric clouds observed by lidar at McMurdo, Antarctica

No.98-14
Mette Dahl Mortensen: The back-propagation method for inversion of radio occultation data

No. 98-15
Xiang-Yu Huang: Variational analysis using spatial filters

No. 99-1
Henrik Feddersen: Project on prediction of climate variations on seasonel to interannual time-scales (PROVOST) EU contract ENVA4-CT95-0109: DMI contribution to the final report: Statistical analysis and post-processing of uncoupled PROVOST simulations

No. 99-2
Wilhelm May: A time-slice experiment with the ECHAM4 A-GCM at high resolution: the experimental design and the assessment of climate change as compared to a greenhouse gas experiment with ECHAM4/OPYC at low resolution

No. 99-3
Niels Larsen et al.: European stratospheric monitoring stations in the Artic II: CEC Environment and Climate Programme Contract ENV4-CT95-0136. DMI Contributions to the project

No. 99-4
Alexander Baklanov: Parameterisation of the deposition processes and radioactive decay: a review and some preliminary results with the DERMA model

No. 99-5
Mette Dahl Mortensen: Non-linear high resolution inversion of radio occultation data

No. 99-6
Stig Syndergaard: Retrieval analysis and methodologies in atmospheric limb sounding using the GNSS radio occultation technique

No. 99-7
Jun She, Jacob Woge Nielsen: Operational wave forecasts over the Baltic and North Sea

No. 99-8
Henrik Feddersen: Monthly temperature forecasts for Denmark - statistical or dynamical?

No. 99-9
P. Thejll, K. Lassen: Solar forcing of the Northern hemisphere air temperature: new data

No. 99-10
Torben Stockflet Jørgensen, Aksel Walløe Hansen: Comment on "Variation of cosmic ray flux and global coverage - a missing link in solar-climate relationships" by Henrik Svensmark and Eigil Friis-Christensen

No. 99-11
Mette Dahl Meincke: Inversion methods for atmospheric profiling with GPS occultations

No. 99-12
Hans-Henrik Benzon; Laust Olsen; Per Høeg: Simulations of current density measurements with a Faraday Current Meter and a magnetometer

No. 00-01
Per Høeg; G. Leppelmeier: ACE - Atmosphere Climate Experiment

No. 00-02
Per Høeg: FACE-IT: Field-Aligned Current Experiment in the Ionosphere and Thermosphere

No. 00-03
Allan Gross: Surface ozone and tropospheric chemistry with applications to regional air quality modeling. PhD thesis

No. 00-04
Henrik Vedel: Conversion of WGS84 geometric heights to NWP model HIRLAM geopotential heights

No. 00-05
Jérôme Chenevez: Advection experiments with DMI-Hirlam-Tracer
No. 00-06
Niels Larsen: Polar stratospheric clouds micro-physical and optical models

No. 00-07
Alix Rasmussen: "Uncertainty of meteorological parameters from DMI-HIRLAM"

No. 00-08
A.L. Morozova: Solar activity and Earth's weather. Effect of the forced atmospheric transparency changes on the troposphere temperature profile studied with atmospheric models

No. 00-09
Niels Larsen, Bjørn M. Knudsen, Michael Gauss, Giovanni Pitari: Effects from high-speed civil traffic aircraft emissions on polar stratospheric clouds

No. 00-10
Søren Andersen: Evaluation of SSM/I sea ice algorithms for use in the SAF on ocean and sea ice, July 2000

No. 00-11
Claus Petersen, Niels Woetmann Nielsen: Diagnosis of visibility in DMI-HIRLAM

No. 00-12
Erik Buch: A monograph on the physical oceanography of the Greenland waters

No. 00-13
M. Steffensen: Stability indices as indicators of lightning and thunder

No. 00-14
Bjarne Amstrup, Kristian S. Mogensen, Xiang-Yu Huang: Use of GPS observations in an optimum interpolation based data assimilation system

No. 00-15
Mads Hvid Nielsen: Dynamisk beskrivelse og hydrografisk klassifikation af den jyske kyststrøm

No. 00-16
Kristian S. Mogensen, Jess U. Jørgensen, Bjarne Amstrup, Xiaohua Yang and Xiang-Yu Huang: Towards an operational implementation of HIRLAM 3D-VAR at DMI

No. 00-17
Sattler, Kai; Huang, Xiang-Yu: Structure function characteristics for 2 meter temperature and relative humidity in different horizontal resolutions

No. 00-18
Niels Larsen, Ib Steen Mikkelsen, Bjørn M. Knudsen m.fl.: In-situ analysis of aerosols and gases in the polar stratosphere. A contribution to THESEO. Environment and climate research programme. Contract no. ENV4-CT97-0523. Final report

No. 00-19
Amstrup, Bjarne: EUCOS observing system experiments with the DMI HIRLAM optimum interpolation analysis and forecasting system

No. 01-01
V.O. Papitashvili, L.I. Gromova, V.A. Popov and O. Rasmussen: Northern polar cap magnetic activity index PCN: Effective area, universal time, seasonal, and solar cycle variations

No. 01-02
M.E. Gorbunov: Radioholographic methods for processing radio occultation data in multipath regions

No. 01-03
Niels Woetmann Nielsen; Claus Petersen: Calculation of wind gusts in DMI-HIRLAM

No. 01-04
Vladimir Penenko; Alexander Baklanov: Methods of sensitivity theory and inverse modeling for estimation of source parameter and risk/vulnerability areas

No. 01-05
Sergej Zilitinkevich; Alexander Baklanov; Jutta Rost; Ann-Sofi Smedman, Vasiliy Lykosov and Pierluigi Calanca: Diagnostic and prognostic equations for the depth of the stably stratified Ekman boundary layer

No. 01-06
Bjarne Amstrup: Impact of ATOVS AMSU-A radiance data in the DMI-HIRLAM 3D-Var analysis and forecasting system

No. 01-07
Sergej Zilitinkevich; Alexander Baklanov: Calculation of the height of stable boundary layers in operational models

No. 01-08
Vibeke Huess: Sea level variations in the North Sea – from tide gauges, altimetry and modelling
No. 01-09
Alexander Baklanov and Alexander Mahura: Atmospheric transport pathways, vulnerability and possible accidental consequences from nuclear risk sites: methodology for probabilistic atmospheric studies

No. 02-01
Bent Hansen Sass and Claus Petersen:
Short range atmospheric forecasts using a nudging procedure to combine analyses of cloud and precipitation with a numerical forecast model

No. 02-02
Erik Buch: Present oceanographic conditions in Greenland waters

No. 02-03
Bjørn M. Knudsen, Signe B. Andersen and Allan Gross: Contribution of the Danish Meteorological Institute to the final report of SAMMOA. CEC contract EVK2-1999-00315: Spring-to-autumn measurements and modelling of ozone and active species

No. 02-04
Nicolai Kliem: Numerical ocean and sea ice modelling: the area around Cape Farewell (Ph.D. thesis)

No. 02-05
Niels Woetmann Nielsen: The structure and dynamics of the atmospheric boundary layer

No. 02-06
Arne Skov Jensen, Hans-Henrik Benzon and Martin S. Lohmann: A new high resolution method for processing radio occultation data

No. 02-07
Per Høeg and Gottfried Kirchengast: ACE+: Atmosphere and Climate Explorer

No. 02-08
Rashpal Gill: SAR surface cover classification using distribution matching

No. 02-09
Kai Sattler, Jun She, Bent Hansen Sass, Leif Laursen, Lars Landberg, Morten Nielsen and Henning S. Christensen: Enhanced description of the wind climate in Denmark for determination of wind resources: final report for 1363/00-0020: Supported by the Danish Energy Authority

No. 02-10
Michael E. Gorbunov and Kent B. Lauritsen: Canonical transform methods for radio occultation data

No. 02-11
Kent B. Lauritsen and Martin S. Lohmann: Unfolding of radio occultation multi path behavior using phase models